Supporting Informations

for

Effects of a solvatomorphism, of the nature of a chelating ligand synthon and of a counterion on the single crystal XRD structure and SMM properties of the paramagnetic monocapped cobalt(II) tris-pyrazoloximates

Svetlana A. Belova[a,b], Alexander S. Belov[a,b], Anastasia A. Danshina,[a,c] Yan V. Zubavichus[d], Dmitriy Yu. Aleshin,[b] Alexander A. Pavlov[a,e], Nikolay N. Efimov[b], Yan Z. Voloshin[a,b]

[a]Nesmeyanov Institute of Organoelement Compounds, Russian Academy of Sciences, 28-1 Vavilova St., 119334 Moscow, Russia

[b]Kurnakov Institute of General and Inorganic Chemistry of the Russian Academy of Sciences, 31 Leninsky Prosp., 119991 Moscow, Russia

[c]Moscow Institute of Physics and Technology (National Research University), 9 Institutskiy per., 141700 Dolgoprudny, Moscow Region, Russia

[d]Synchrotron Radiation Facility SKIF, Boreskov Institute of Catalysis SB RAS, 630559 Koltsovo, Russia

[e]BMSTU Center of National Technological Initiative “Digital Material Science: New Material and Substances”, Bauman Moscow State Technical University, 2nd Baumanskaya st. 5, 105005 Moscow, Russia

Materials

The reagents used, $CoCl_2 \cdot 6H_2O$, $CoBr_2 \cdot 6H_2O$, phenylboronic and hydroiodic acids, sorbents and organic solvents were obtained commercially (SAF®). The initial solvatocomplex $CoI_2 \cdot 6H_2O$ was obtained by the reaction of $Co(OH)_2$ with aqueous hydroiodic acid, followed by partial evaporation of the reaction mixture, and its cooling to r.t.; the precipitate formed was filtered off and dried in air atmosphere. 3-acetylpyrazoloxime (*PzOxH*) and 3-formylpyrazoloxime (*FPzOxH*) were prepared as described,[S1, S2] respectively.

Analytical and Spectral data

Analytical data (C, H, N contents) for the prepared new compounds were obtained with a Carlo Erba Model 1106 automatic elemental analyzer. Cobalt, bromine and iodine contents were determined using the X-ray fluorescence method.

Their MALDI-TOF mass spectra were recorded with and without of 2,5-dihydroxybenzoic acid as the matrix using a MALDI-TOF-MS Bruker Autoflex II (Bruker Daltonics) mass spectrometer in reflecto-mol mode. The ionization was induced by UV-laser with wavelength 337 nm. The samples were applied to a nickel plate. The accuracy of measurements was 0.1%.

^{1}H NMR spectra of the obtained pseudoclathrochelate complexes were recorded from their solutions in CD_2Cl_2, $CDCl_3$ and benzene-d_6 with a Varian Inova 400 and Bruker Avance 600 spectrometers. The measurements were done using the residual signals of these deuterated solvents.

UV-vis spectra of their solutions in acetonitrile were recorded in the range 220 – 800 nm with a Varian Cary 60 spectrophotometer. The individual Gaussian components of these spectra were calculated using the Fityk program.[S3]

Synthetic protocols, Spectral and Analytical Characteristics

$[Co(FPzOx)_3(BC_6H_5)Cl]$. Phenylboronic acid (0.05 g, 0.43 mmol) and 3-formylpyrazoloxime (0.13 g, 1.17 mmol) were dissolved in ethanol (2 ml) under argon, and $NaHCO_3$ (0.04 g, 0.47 mmol) and $CoCl_2{\cdot}6H_2O$ (0.09 g, 0.39 mmol) were added to the stirring solution. The dark-brown reaction mixture was refluxed under intensive stirring for 30 min and then cooled to r.t. The brown precipitate formed was filtered off, washed with ethanol (6 ml, in two portions), diethyl ether (10 ml, in two portions) and hexane (5 ml). The product was extracted with dichloromethane (4 ml, in two portions) and the combined bright-orange extract was filtered, evaporated to dryness and dried *in vacuo*. Yield: 0.06 g (31%). Found (%): C, 42.15; H, 3.32; N, 24.58; Co, 11.51. Calcd. for $C_{18}H_{17}N_9O_3BClCo$ (%): C, 41.96; H, 3.37; N, 24.42; Co, 11.70. MS(MALDI-TOF): *m/z* (I,%): 366(19) $[Co(FPzOx)_2(BC_6H_5){\cdot}H^+]^+$, 459(59) $[Co(FPzOx)_2(BC_6H_5){\cdot}(CoCl)^+]^+$, 534(100) $\{[Co_2(FPzOx)_3(BC_6H_5)]{\cdot}3H^+\}^+$, 824(27) $\{[Co_2(FPzOx)_4(BC_6H_5)_2Cl^-]{\cdot}Co^{2+}\}^+$. ^1H NMR ($CDCl_3$ + CD_2Cl_2 (3:1) mixture, δ, ppm): −10.62 (br. s, 3H, 4-Pz), 29.23 (br. s, 1H, *para*-Ph), 33.80 (br. s, 2H, *meta*-Ph), 75.23 (br. s, 2H, *ortho*-Ph), 82.19 (br. s, 3H, 5-Pz), 159.75 (br. s, 9H, CH=N), 267.41 (br. s, 3H, NH). Deconvoluted UV-vis (CH_3CN): ν_{max}, cm^{-1} ($\varepsilon \cdot 10^{-3}$, $mol^{-1}\ L\ cm^{-1}$): 40480(21), 39680(13), 37310(1.6), 35590(10), 31250(3.2).

$[Co(PzOx)_3(BC_6H_5)Cl]$. Phenylboronic acid (0.12 g, 1.0 mmol) and 3-acetylpyrazoloxime (0.40 g, 3.1 mmol) were dissolved in ethanol (10 ml) under argon, and $NaHCO_3$ (0.23 g, 2.7 mmol) and $CoCl_2{\cdot}6H_2O$ (0.1 g, 0.90 mmol) were added to the stirring solution. The orange precipitate has been formed. The reaction mixture was refluxed under intensive stirring for 30 min and then cooled to r.t. The precipitate was filtered off, washed with ethanol (20 ml, in four portions) and diethyl ether (10 ml, in two portions), and extracted with chloroform (10 ml, in two portions). The combined

extract was filtered, evaporated to dryness and dried *in vacuo*. Yield: 0.42 g (84%).

The analytical and spectral data for this product were identical to those earlier described.[S4]

[Co(PzOx)$_3$(BC$_6$H$_5$)Br]. Phenylboronic acid (0.12 g, 1.0 mmol) and 3-acetylpyrazoloxime (0.37 g, 2.9 mmol) were dissolved in ethanol (10 ml) under argon, and $NaHCO_3$ (0.14 g, 1.7 mmol) and $CoBr_2 \cdot 6H_2O$ (0.27 g, 0.84 mmol) were added to the stirring solution. The orange precipitate has been formed. The reaction mixture was refluxed under intensive stirring for 30 min and then cooled to r.t. The precipitate was filtered off, washed with ethanol (20 ml, in three portions) and diethyl ether (7 ml), and extracted both with acetonitrile (30 ml, in four portions) and with THF (30 ml, in four portions). The combined extract was filtered, evaporated to dryness and dried *in vacuo*. Yield: 0.26 g (52%). Found (%): C, 41.95; H, 3.36; N, 24.41; Co, 11.75. Calcd. for $C_{21}H_{23}N_9O_3BBrCo$ (%): C, 42.15; H, 3.32; N, 24.58; Co, 11.51. MS(MALDI-TOF): *m/z* (I,%) (without matrix): 394(100) $[Co(PzOx)_2(BC_6H_5)\cdot H^+]^+$, 532(16) $[Co(PzOx)_2(BC_6H_5)\cdot(CoBr)^+]^+$, 576(81) $\{[Co_2(PzOx)_3(BC_6H_5)]\cdot 3H^+\}^+$, 924(64) $\{[Co_2(PzOx)_4(BC_6H_5)_2Br]^-\cdot Co^{2+}\}^+$; (DHB matrix): 519 $[Co(PzOx)_3(BC_6H_5)]^+$. ^{1}H NMR (benzene-d_6, δ, ppm): −14.75 (br. s, 9H, CH_3), −9.96 (br. s, 3H, 4-Pz), 29.32 (br. s, 1H, *para*-Ph), 34.40 (br. s, 2H, *meta*-Ph), 78.56 (br. s, 2H, *ortho*-Ph), 84.74 (br. s, 3H, 5-Pz), 269.98 (br. s,3H, NH). Deconvoluted UV-vis (CH_3CN): ν_{max}, cm^{-1} ($\varepsilon \cdot 10^{-3}$, mol^{-1} L cm^{-1}): 40650(23), 40320(5.2), 35840(8.2), 32150(3.4).

[Co(PzOx)$_3$(BC$_6$H$_5$)I]. Phenylboronic acid (0.11 g, 0.93 mmol) and 3-acetylpyrazoloxime (0.34 g, 2.7 mmol) were dissolved in ethanol (10 ml) under argon, and $NaHCO_3$ (0.26 g, 6.2 mmol) and $CoI_2 \cdot 2H_2O$ (0.27 g, 0.77 mmol) were added to the stirring solution. The orange precipitate has been formed. The reaction mixture was refluxed under intensive stirring for

15 min and then cooled to r.t. The precipitate was filtered off, washed with ethanol (30 ml, in four portions) and extracted with THF (16 ml, in four portions). The combined extract was filtered, evaporated to dryness and dried *in vacuo*. Yield: 0.41 g (82%). Found (%): C, 39.12; H, 3.75; N, 19.25; Co, 8.00; I, 11.26. Calcd. for $C_{21}H_{23}N_9O_3BICo$ (%): C, 39.01; H, 3.56; N, 19.51; Co, 8.13; I, 11.08. MS(MALDI-TOF): *m/z* (I,%) (without matrix): 394(72) $[Co(PzOx)_2(BC_6H_5)\cdot H^+]^+$, 576(100) $\{[Co_2(PzOx)_3(BC_6H_5)]\cdot 3H^+\}^+$, 972(70) $\{[Co_2(PzOx)_4(BC_6H_5)_2I]^-\cdot Co^{2+}\}^+$; (DHB matrix): 519 $[Co(PzOx)_3(BC_6H_5)]^+$. ^{1}H NMR (benzene-d_6, δ, ppm): −14.42 (br. s, 9H, CH_3), −10.03 (br. s, 3H, 4-Pz), 29.07 (br. s, 1H, *para*-Ph), 34.11 (br. s, 2H, *meta*-Ph), 78.04 (br. s, 2H, *ortho*-Ph), 84.30 (br. s, 3H, 5-Pz), 266.53 (br. s, 3H, NH). Deconvoluted UV-vis (CH_3CN): ν_{max} , cm^{-1} ($\varepsilon \cdot 10^{-3}$, mol^{-1} L cm^{-1}): 40650(31), 40000(4.7), 36760(11), 34720(2.9), 33000(4.7).

Synthesis

Comparing *PzOxH versus FPzOxH* as the pyrazoloxime chelating synthons for assembly of their phenylboron-monocapped chloride-H-bonded cobalt(II) complexes, we found that the derivative of the former methyl-containing 3-acetylpyrazoloxime has been formed in the substantially higher yield than that of its methine-containing analog (*i.e.*, *PzOxH* is a more efficient chelating synthon), due to the electronodonor effect of methyl substituent increasing a *N*-donor ability of its oxime group. Their less *N*-donor analog with electronoacceptor trifluoromethyl group do not form a cobalt(II) complexes of this type.

It should be noted that even in the presence of 10^4 – 10^5 excesses of bromide or iodide anions, Cl^- ion is a more efficient pseudocapping H-acceptor agent for the three pyrazole groups of the covalently bound boron-monocapped cation $[Co(PzOx)_3(BC_6H_5)]^+$. Moreover, even a crystallization of the initially formed cobalt(II) pseudoclathrochelates of this type with H-

bonded Br^- or I^- counteranions from the chlorine-containing solvents, such as chloroform or dichloromethane, can cause an exchange of these apical halogenide anions by Cl^- ion that realizes in a course of photochemical transformations of the aforementioned media (chloride anions are known [S5] to result, in particular, from a formation of phosgene $COCl_2$ and from the corresponding radical species as well). Such radical processes and exchange reactions have been earlier observed [S6] even in the clathrochelate chemistry (keeping in mind that the macrobicyclic metal complexes of this class of coordination compounds typically possess an unprecedent chemical robustness even in harsh acidic media [S7]). Among their more reactive pseudoclathrochelate analogs, such chloride-induced exchange reaction has been recently observed [S8] for the DMF-capped cobalt(II) complex **2** shown in Chart 1 in a course of its ^{1}H NMR titration with $((n\text{-}C_4H_9)_4N)Cl$ in acetonitrile-d_3 as a solvent.

The yields of the target semiclathrochelate derivatives of PzOxH and of FPzOxH are equal to 84% and to 31%, respectively. This result can be explained by a well-known [S9] electronodonor effect of methyl substituent in the molecule *PzOxH*, the presence of which causes an increase in the *N*-donor ability of its oxime group. As a result, such strongly "antientropic", but enthalpy driven, self-assembly of a pseudomacrobicyclic intracomplex molecule with three π-conjugated five-membered chelate C=N–Co–N=C cycles, three six-membered B–O–N–Co–N–O cycles with ordinary covalent and coordination bonds, and three H-bonded six-membered Hal^-…HN–N–Co–N–NH pseudochelating moieties as well, is observed. Indeed, our attempts to perform the same coordination-driven template reaction using their trifluoromethyl-substituted analog, also shown in Scheme 1, as a chelating ligand synthon with a more lower donor ability (due to the presence of strong electron-withdrawing fluoroalkyl substituent in its oximate fragment), thus trying to further decrease a ligand field strength,

were unsuccessful. We also unexpectedly observed that the solubility of a pseudoclathrochelate derivative of the methine-containing synthon *FPzOxH*, the cobalt(II) complex $[Co(FPzOx)_3(BC_6H_5)Cl]$, is higher in dichloromethane than in chloroform. Indeed, the metal pseudoclathrochelates of this type typically possess an opposite order of their solubility in these solvents.

X-ray crystallography

In the solvates of the methyl-containing complex $[Co(PzOx)_3(BC_6H_5)Cl]$ with three different solvents, benzene, chloroform and acetone (Figs S2 – S4), there is a clear tendency for the distortion angle φ to decrease from 2.7(3)° in $[Co(PzOx)_3(BC_6H_5)Cl]\cdot(CH_3)_2CO$ to 0.47(13)° in $[Co(PzOx)_3(BC_6H_5)Cl]\cdot CHCl_3$ [S4, S10] (Table S2). In the latter, the average Co–N bond lengths are the longest (2.163(3)Å) while in $[Co(PzOx)_3(BC_6H_5)Cl]\cdot C_6H_6$ and $[Co(PzOx)_3(BC_6H_5)Cl]\cdot(CH_3)_2CO$, they are hardly affected by the presence of a lattice solvent (av. Co–N 2.141(2) and 2.145(2)Å, respectively). The solvate with chloroform also features the longest N–H…Cl hydrogen bonds (Table S2), thereby mirroring the tendency observed between the clathrochelate homologs with and without methyl groups in the encapsulating ligand. In the mixed crystal $\{[Co(PzOx)_3(BC_6H_5)I]_{0.69}[Co(PzOx)_3(BC_6H_5)Cl]_{0.31}\}\cdot C_6H_6$ (Fig. S1), the distortion angle φ becomes lower (0.77(15)°) than in the chloride-H-bonded complex with the same solvent, $[Co(PzOx)_3(BC_6H_5)Cl]\cdot C_6H_6$ (1.29(8)°), while the average Co–N bond length is nearly the same (2.146(3) Å). In contrast, the hydrogen bonds to the chloride anion that has the minor occupancy (0.31 *vs.* 0.69) are the weakest among the solvatomorphs of the chloride-containing clathrochelate (N…Cl 3.222(12) – 3.333(14) Å, NHCl 168.3(3) – 173.8(4)°). The hydrogen bonds to the iodide anion (N…I 3.428(2) – 3.631(3) Å, NHI 171.10(20) – 176.91(16)°), however, are similar

to those in the solvent-free crystal of $[Co(PzOx)_3(BC_6H_5)I]$ (N…I 3.558(10) – 3.576(9) Å, NHI 150.3(6) – 168.3(5)°; Fig. S8). The same is also true for the average Co–N bond length, which is 2.149(8) Å but the distortion angle φ increases to 3.8(5)° (Table S2).

In the benzene-containing solvatomorph of its bromide-H-bonded analog $[Co(PzOx)_3(BC_6H_5)Br]$ (Fig. S5), the angle φ is as low as 2.54(5)° and the average Co–N bond length is 2.162(3) Å. The hydrogen bonds to Br^- anion are expectedly stronger than in the above iodide-containing complexes (N…Br 3.279(3) – 3.396(3) Å, NHBr 169.9(2) – 173.9(2)°). In the tetrahydrofuran-containing solvatomorph, $[Co(PzOx)_3(BC_6H_5)Br]\cdot THF$ (Fig. S6), both the distortion angle φ and the average Co-N bond length decrease (1.2(3)° and 2.145(4) Å; Table S2) while the hydrogen bonds to bromide anion remain almost the same (N…Br 3.237(5) – 3.384(4) Å, NHBr 170.9(3) – 175.0(2)°).

Mass spectra

Their MALDI-TOF mass spectra measured with 2,5-dihydroxybenzoic acid as a matrix, contain the low intensive peaks of the complex cations $[Co(PzOx)_3(BC_6H_5)]^+$ or $[Co(FPzOx)_3(BC_6H_5)]^+$. In the positive range of the spectra of the 3-acetylpyrazoloxime derivatives measured without this matrix, the substantially more intensive peaks of the fragmental and clusters cations $[Co(PzOx)_2(BC_6H_5)\cdot H^+]^+$, $\{[Co_2(PzOx)_3(BC_6H_5)]\cdot 3H^+\}^+$, $[Co(PzOx)_2(BC_6H_5)\cdot(CoHal)^+]^+$ and $\{[Co_2(PzOx)_4(BC_6H_5)_2Hal^-]\cdot Co^{2+}\}^+$ are observed. The analogous peaks are observed in the spectrum of their tris-methine-containing analog $[Co(FPzOx)_3(BC_6H_5)Cl]$. These complex species resulted from a heterolytic dissociation of the corresponding molecular ions and such fragmentation processes are characteristic of the boron-monocapped metal(II) tris-pyrazoloximates.[S11] The experimentally observed isotopic distributions in these peaks are in good agreement with the

theoretically calculated models for the aforementioned fragmental and cluster cations.

UV-vis spectra

Deconvoluted solution UV-vis spectra of the obtained cobalt(II) tris-pyrazoloximates (Figs. S10–S13 and Table S3) contain a series of the intensive bands in the UV range assigned the cobalt(II)-centered metal-to-ligand charge transfers (MLCTs) Co$d^7 \rightarrow$Lπ^* and to the allowed intraligand π–π^* transitions in the chelating pyrazoloximate fragments and in the phenyl apical substituent at the single capping boron atom as well. The performed comparison of the deconvoluted UV-spectra of the initial chelating and cross-linking ligand synthons (Figs. S14–S17) and those of their cobalt(II)-centered pseudoclathrochelate derivatives allowed to observe an appearance of two or three intense ($\varepsilon \sim 1 \div 10 \cdot 10^3$ mol^{-1} L cm^{-1}) bands in the near-UV range with maxima from 30000 to 37000 cm^{-1} after a coordination-driven self-assembly of the aforementioned synthons on the cobalt(II) ion as a matrix. Therefore, these bands were assigned to the MLCTs Co$d^7 \rightarrow$Lπ^*.

Calculation of magnetometry data

Magnetic susceptibility data at the constant field of 5 kOe complied in Table S4 were fitted using the PHI [S12] program with the following Hamiltonian:

$$\hat{H} = -\sigma\lambda\hat{L}\hat{S} + \Delta\left(3\hat{L}_z^2 - \hat{L}^2\right) + \delta(\hat{L}_+^2 - \hat{L}_-^2) + \mu_\beta(-\sigma\hat{L} + g_e\hat{S})B \quad (1)$$

where σ is the orbital reduction factor; λ is the constant of spin-orbital coupling; Δ is a parameter describing the splitting of T sate; δ is a parameter describing the splitting of E state; g_e is the free electron g-factor; B is the magnetic field; $\hat{L}$,$\hat{S}$ are the orbital and spin momentum operators; μ_β is Bohr magneton.

The zero-field splitting model did not allow to well describe the experimental magnetic susceptibility data. Therefore, they were fitted by Griffith model, taking into account the unquenched orbital momentum of cobalt(II) ion. The values of magnetic susceptibility for the complexes $[Co(FPzOx)_3(BC_6H_5)Cl]$ and $[Co(PzOx)_3(BC_6H_5)Cl] \cdot (CH_3)_2CO$ in the high-temperature range were higher than the spin-only value of approximately 3.15 cm^3K/mol thus suggesting a substantial amount of the unquenched orbital moment. In the case of the complexes $[Co(PzOx)_3(BC_6H_5)I]$, $[Co(PzOx)_3(BC_6H_5)]Br$ and $[Co(PzOx)_3(BC_6H_5)Cl]$, these values are more close to spin-only magnitude. Nevertheless, the corresponding values of magnetic susceptibility at 100 K for the clathrochelates $[Co(PzOx)_3(BC_6H_5)I]$ and $[Co(PzOx)_3(BC_6H_5)]Br$ are higher than those at room temperature, thus suggesting a population of the state with a higher magnetic moment [F.Lloret, M.Julve, J.Cano, R.Ruiz-Garcia, E.Pardo, Magnetic properties of six-coordinated high-spin cobalt(II) complexes: Theoretical background and its application, *Inorg.Chim.Acta*, 2008, 361, 3432–3445, DOI: 10.1016/j.ica.2008.03.114]. It should be noted that the fine-crystalline samples under study were immobilized on a mineral oil matrix inside a polyethylene capsule in order to prevent a field-induced orientation. Indeed, this excludes the latter effect caused by the orientation of the fine-crystalline samples under study in the direction of χ_{zz}. In the applied model, the axial splitting parameter Δ describes a splitting of T state that is observed in passing from the octahedral O_h-geometry of a free Co^{2+} ion to the TP D_{3h}-symmetric CoN_6-coordination polyhedron of the encapsulated cobalt(II) ion. Aiming to take into account a distortion of this TP geometry, the δ parameter that describes a splitting of E term was included in the Griffith model. The spin-orbit coupling constant for a free Co^{2+} ion is approximately -170 cm^{-1}; this value is known [F.Lloret, M.Julve, J.Cano, R.Ruiz-Garcia, E.Pardo, Magnetic properties of six-coordinated high-spin cobalt(II) complexes: Theoretical background and its application, *Inorg.Chim.Acta*, 2008, 361, 3432–3445, DOI: 10.1016/j.ica.2008.03.114] to decrease for its complexes. Indeed, modules of the obtained values of spin-orbit coupling constant for the

cobalt(II) clathrochelates under study are lower than that for a free Co^{2+} ion. The orbital reduction factor was included in the used model in order to take into account an admixture of the low-lying triplet and overlying P term.

The obtained values of orbital reduction factor σ (see SI, Table S4) fall in the range 1.38 – 1.63, thus being a slightly higher than those estimated which typically ranged from 1 to 1.5 [F.Lloret, M.Julve, J.Cano, R.Ruiz-Garcia, E.Pardo, Magnetic properties of six-coordinated high-spin cobalt(II) complexes: Theoretical background and its application, *Inorg.Chim.Acta*, 2008, 361, 3432–3445, DOI: 10.1016/j.ica.2008.03.114]. Nevertheless, the attempted fitting with a fixed σ value of 3/2 did not allowed to correctly describe the obtained experimental data in all the temperature range (see SI section).

AC magnetometry data were fitted using the following Cole–Cole equations:

$$\chi'(\vartheta) = \chi_S + (\chi_T - \chi_S)\frac{1 + (\vartheta\tau)^{1-\alpha}sin(^{\pi\alpha}/_2)}{1 + 2(\vartheta\tau)^{1-\alpha}sin\left(^{\pi\alpha}/_2\right) + (\vartheta\tau)^{2-2\alpha}} \quad (2)$$

$$\chi''(\vartheta) = (\chi_T - \chi_S)\frac{(\vartheta\tau)^{1-\alpha}cos(^{\pi\alpha}/_2)}{1 + 2(\vartheta\tau)^{1-\alpha}sin\left(^{\pi\alpha}/_2\right) + (\vartheta\tau)^{2-2\alpha}} \quad (3)$$

where χ_T, χ_S is the isothermal and the adiabatic susceptibilities, respectively; ϑ is the frequency of AC modulation field; τ is the relaxation time; α is a parameter describing the number of relaxation ways.
were fitted in good quality using the single independent function, while the correct approximation of those for the clathrochelates $[Co(PzOx)_3(BC_6H_5)Br]$ and $[Co(PzOx)_3(BC_6H_5)I]$ could be performed only using two independent functions.

Relaxation times were fitted simultaneously for 0 Oe and 1000 Oe applied field according to equation 4. For complexes $[Co(PzOx)_3(BC_6H_5)Br]$, $[Co(PzOx)_3(BC_6H_5)I]$ with two independent peaks at 0 Oe for fitting procedure were taken low-frequency ones since for high

temperatures the dependencies for 1000 Oe and 0 Oe have similar behavior that display same contributions from Orbach and Raman mechanisms.

$$\tau^{-1} = \frac{B_1}{1 + B_1 H^2} + AH^n T + CT^m + \tau_0^{-1} e^{-U/kT} \quad (4)$$

Table S1. Crystal data and structure refinement parameters for the complexes $[Co(PzOx)_3(BC_6H_5)Cl]\cdot CHCl_3$, $[Co(PzOx)_3(BC_6H_5)Cl]$, $[Co(PzOx)_3(BC_6H_5)Cl]\cdot(CH_3)_2CO$, $[Co(PzOx)_3(BC_6H_5)Cl]\cdot C_6H_6$, $[Co(FPzOx)_3(BC_6H_5)Cl]$, $\{[Co(PzOx)_3(BC_6H_5)I]_{0.69}[Co(PzOx)_3(BC_6H_5)Cl]_{0.31}\}\cdot C_6H_6$, $[Co(PzOx)_3(BC_6H_5)I]$, $[Co(PzOx)_3(BC_6H_5)Br]\cdot THF$ and $[Co(PzOx)_3(BC_6H_5)Br]\cdot C_6H_6$

Parameter	**$[Co(PzOx)_3(BC_6H_5)Cl]\cdot CHCl_3$**	**$[Co(PzOx)_3(BC_6H_5)Cl]$**	**$[Co(PzOx)_3(BC_6H_5)Cl]\cdot(CH_3)_2CO$**	**$[Co(PzOx)_3(BC_6H_5)Cl]\cdot C_6H_6$**	**$[Co(FPzOx)_3(BC_6H_5)Cl]$**	**$\{[Co(PzOx)_3(BC_6H_5)I]_{0.69}[Co(PzOx)_3(BC_6H_5)Cl]_{0.31}\}\cdot C_6H_6$**	**$[Co(PzOx)_3(BC_6H_5)I]$**	**$[Co(PzOx)_3(BC_6H_5)Br]\cdot THF$**	**$[Co(PzOx)_3(BC6H5)Br]\cdot C_6H_6$**
Empirical formula	$C_{22}H_{24}BCl_4CoN_9O_3$	$C_{21}H_{23}BClCoN_9O_3$	$C_{24}H_{29}BClCoN_9O_4$	$C_{27}H_{29}BClCoN_9O_3$	$C_{18}H_{17}BClCoN_9O_3$	$C_{27}H_{29}BCl_{0.31}CoI_{0.69}N_9O_3$	$C_{21}H_{23}BICoN_9O_3$	$C_{25}H_{31}BBrCoN_9O_4$	$C_{27}H_{29}BBrCoN_9O_3$
Formula weight	674.04	554.67	612.75	632.78	512.59	695.88	646.12	671.24	677.24
T, K	100	100	120	100	120	120	120	120	100
Crystal system	Monoclinic	Monoclinic	Triclinic	Triclinic	Monoclinic	Triclinic	Monoclinic	Triclinic	Triclinic
Space group	$P2_1/n$	$P2_1/c$	P-1	P-1	$P2_1/c$	P-1	$P2_1/c$	P-1	P-1
Z	4	4	2	2	4	2	4	2	2
a, Å	8.3209(17)	15.744(3)	8.096(2)	8.1600(16)	9.1009(7)	8.2151(6)	8.7090(17)	8.1745(16)	8.2500(16)
b, Å	19.369(4)	8.1571(16)	10.116(3)	13.400(3)	14.2006(10)	13.4093(10)	28.144(6)	13.088(3)	13.319(3)
c, Å	18.121(4)	18.785(4)	18.105(5)	13.690(3)	16.7978(12)	14.4049(10)	10.552(2)	14.139(3)	14.251(3)
a, °	90	90	78.627(6)	92.98(3)	90	87.978(2)	90	89.31(3)	89.48(3)
b, °	95.84(3)	95.17(3)	77.176(6)	102.15(3)	100.580(2)	74.903(2)	99.775(4)	75.61(3)	74.35(3)
γ, °	90	90	80.835(6)	96.45(3)	90	75.460(2)	90	78.60(3)	76.82(3)
V, Å^3	2905.5(10)	2402.7(8)	1406.9(6)	1449.7(5)	2134.0(3)	1482.22(19)	2548.8(9)	1435.2(5)	1465.8(6)
D_{calc} (g·cm^{-3})	1.541	1.533	1.446	1.450	1.595	1.559	1.684	1.553	1.534
Linear absorption, μ (cm^{-1})	23.87	12.15	7.53	9.86	9.72	13.71	19.27	20.39	18.97
F(000)	1372	1140	634	654	1044	704	1284	686	690
$2\Theta_{max}$, °	77.1	58	58	60	60	56	50	54	76.9
Reflections measured	15044	13505	15903	21240	27147	17100	22802	20076	25384
Independent reflections	6162	4385	7435	6059	6214	7141	4497	6260	6045
Observed reflections [I>2σ(I)]	3669	4082	4758	5463	4931	5219	2709	3436	4601
Parameters	365	329	366	401	298	392	323	389	383
R1	0.0742	0.0443	0.0775	0.0326	0.0359	0.0400	0.0749	0.0555	0.0653
wR2	0.1740	0.1117	0.2351	0.0894	0.0848	0.0922	0.2241	0.1247	0.1766
GOF	0.950	1.063	1.079	1.029	1.022	1.026	1.021	0.949	1.081
$\Delta\rho_{max}$/ $\Delta\rho_{min}$ (e Å^{-3})	0.886/-0.986	0.612/-0.432	1.217/-1.203	0.278/-0.321	0.588/-0.301	0.663/-0.415	1.107/-1.945	0.896/-0.757	1.076/-1.383

Table S2. Selected geometrical parameters of the intracomplex pseudoclathrochelate molecules in the crystals **[**$Co(PzOx)_3(BC_6H_5)Cl]\cdot CHCl_3$, $[Co(PzOx)_3(BC_6H_5)Cl]$, **[**$Co(PzOx)_3(BC_6H_5)Cl]\cdot(CH_3)_2CO$, **[**$Co(PzOx)_3(BC_6H_5)Cl]\cdot C_6H_6$, **[**$Co(FPzOx)_3(BC_6H_5)Cl]$, **[**$Co(PzOx)_3(BC_6H_5)I]$+$[Co(PzOx)_3(BC_6H_5)Cl]\cdot C_6H_6$, $[Co(PzOx)_3(BC_6H_5)I]$, $[Co(PzOx)_3(BC_6H_5)Br]\cdot$THF and $[Co(PzOx)_3(BC_6H_5)Br]\cdot C_6H_6$.

Parameter	**[Co(PzOx)$_3$(BC$_6$H$_5$)Cl]·CHCl$_3$**	**[Co(PzOx)$_3$(BC$_6$H$_5$)Cl]**	**[Co(PzOx)$_3$(BC$_6$H$_5$)Cl]·(CH$_3$)$_2$CO**	**[Co(PzOx)$_3$(BC$_6$H$_5$)Cl]·C$_6$H$_6$**	**[Co(FPzOx)$_3$(BC$_6$H$_5$)Cl]**	**[Co(PzOx)$_3$(BC$_6$H$_5$)I]+ [Co(PzOx)$_3$(BC$_6$H$_5$)Cl]·C$_6$H$_6$***	**[Co(PzOx)$_3$(BC$_6$H$_5$)I]**	**[Co(PzOx)$_3$(BC$_6$H$_5$)Br]·THF**	**[Co(PzOx)$_3$(BC$_6$H$_5$)Br]·C$_6$H$_6$**
Anion	Cl^-	Cl^-	Cl^-	Cl^-	Cl^-	I^-/Cl^- (69:31)	I^-	Br^-	Br
Solvent	$CHCl_3$	-	acetone	benzene	-	benzene	-	THF	benzene
Co – N1 (Å)	2.166(3)	2.136(2)	2.112(4)	2.130(2)	2.148(2)	2.149(2)	2.140(8)	2.151(4)	2.145(3)
Co – N2 (Å)	2.151(4)	2.167(2)	2.165(4)	2.141(1)	2.148(2)	2.161(3)	2.143(8)	2.164(4)	2.180(4)
Co – N4 (Å)	2.142(3)	2.164(2)	2.165(4)	2.138(2)	2.145(2)	2.119(3)	2.152(8)	2.117(5)	2.163(3)
Co – N5 (Å)	2.179(3)	2.130(2)	2.139(4)	2.142(2)	2.147(1)	2.154(2)	2.144(9)	2.162(4)	2.182(3)
Co – N7 (Å)	2.153(3)	2.114(2)	2.135(4)	2.138(1)	2.126(2)	2.126(2)	2.124(8)	2.141(4)	2.135(3)
Co – N8 (Å)	2.184(3)	2.151(2)	2.153(4)	2.154(2)	2.149(2)	2.169(3)	2.188(9)	2.162(5)	2.165(3)
N – O (Å)	1.379(4) -1.389(4) *av.* 1.383	1.370(3) - 1.381(3) *av.* 1.376	1.369(5) - 1.377(5) *av.* 1.374	1.370(2) - 1.378(2) *av.* 1.374	1.365(2) - 1.374(2) *av.* 1.371	1.373(3) - 1.384(3) *av.* 1.379	1.376(9) - 1.388(9) *av.* 1.381	1.376(5) - 1.383(5) *av.* 1.380	1.384(4) - 1.391(4) *av.* 1.387
B – O (Å)	1.501(4) -1.516(4) *av.* 1.507	1.488(3) - 1.495(3) *av.* 1.492	1.478(7) - 1.504(6) *av.* 1.495	1.488(3) - 1.494(2) *av.* 1.490	1.482(3) - 1.504(2) *av.* 1.495	1.491(5) - 1.500(3) *av.* 1.495	1.48(1) - 1.50(1) *av.* 1.49	1.489(7) - 1.507(7) *av.* 1.499	1.491(5) - 1.502(5) *av.* 1.497
C=N (Å)	1.296(5) - 1.366(5) *av.* 1.331	1.280(3) - 1.346(3) *av.* 1.313	1.283(7) - 1.349(6) *av.* 1.319	1.284(2) - 1.343(3) *av.* 1.314	1.276(2) - 1.348(2) *av.* 1.312	1.282(4) - 1.354(3) *av.* 1.318	1.27(1) - 1.34(1) *av.* 1.30	1.288(7) - 1.359(6) *av.* 1.321	1.291(5) - 1.358(5) *av.* 1.325
C – C (Å)	1.464(5)-1.466(5) *av.* 1.465	1.457(3) - 1.464(3) *av.* 1.459	1.458(7) - 1.466(7) *av.* 1.463	1.453(3) - 1.462(2) *av.* 1.457	1.451(3) - 1.461(3) *av.* 1.454	1.458(4) - 1.468(4) *av.* 1.464	1.46(1) - 1.48(1) *av.* 1.47	1.454(7) - 1.462(7) *av.* 1.458	1.469(5) - 1.475(5) *av.* 1.471
N=C – C=N (°)	0.1(5) - 2.3(4) *av.* 4.6	0.4(4) - 3.1(3) *av.* 1.8	1.1(7) - 3.0(7) *av.* 2.1	2.2(2) - 4.0(2) *av.* 3.3	0.3(3) - 2.7(2) *av.* 1.8	0.4(4) - 1.6(4) *av.* 1.1	1(1) - 4(1) *av.* 2	1.1(7) - 3.6(7) *av.* 2.0	0.9(5) – 3.3(5) *av.* 1.5
NH…anion (Å)	3.139(4) - 3.194(3)	3.094(2) - 3.136(2)	3.099(4) – 3.175(4)	3.068(2) -3.192(2)	3.1111(18) - 3.1838(18)	3.428(2) - 3.631(3) [3.222(12)-3.333(14)]	3.558(10) - 3.576(9)	3.237(5) - 3.384(4)	3.279(3) - 3.396(3)
∠NH – anion (°)	170.28(19) - 171.8(2)	167.90(15) - 171.68(14)	163.8(3) - 167.7(3)	168.21(11) - 174.82(11)	167.43(10) -179.63(11)	171.10(20)-176.91(16) [168.3(3)-173.8(4)]	150.3(6) – 168.3(5)	170.9(3) – 175.0(2)	169.9(2)-173.9(2)
φ (°)	0.47(13)	3.01(10)	2.7(3)	1.29(8)	1.17(8)	0.77(15)	3.8(5)	1.2(3)	2.54(5)
h (Å)	2.602(3)	2.5738(18)	2.582(3)	2.5665(14)	2.5840(13)	2.572(2)	2.573(6)	2.572(3)	2.591(2)
Co…anion (Å)	4.723(5)	4.6327(5)	4.6600(18)	4.6287(18)	4.6839(6)	5.1361(7) [4.844(12)]	5.1745(16)	4.848(2)	4.8874(19)

*In the brackets, the values for Cl^--counteranion having a minor occupancy.

Table S3. Maxima (ν, cm^{-1}) and intensities ($\varepsilon \cdot 10^{-3}$, $mol^{-1}\,L\,cm^{-1}$) of the bands in the deconvoluted UV-vis spectra of the acetonitrile solutions of the cobalt(II) complexes under study and those of the initial ligand synthons in their ethanol solutions

Compound	ν_1	ν_2	ν_3	ν_4	ν_5	ν_6	ν_7	ν_8	ν_9
FPzOxH				43105(8.8)	40160(4.6)			32573(0.086)	
PzOxH				42735(11)	39840(3.0)	38315(0.78)			
$[Co(FPzOx)_3(BC_6H_5)Cl]$				40480(21)	39680(13)	37310(1.6)	35590(10)	31250(3.2)	
$[Co(PzOx)_3(BC_6H_5)Cl]$				41150(13)	40320(4.2)	37170(12)		31650(1.1)	30210(1.3)
$[Co(PzOx)_3(BC_6H_5)Br]$				40650(23)	40320(5.2)		35840(8.2)	32150(3.4)	
$[Co(PzOx)_3(BC_6H_5)I]$				40650(31)	40000(4.7)		36760(11)	34720(2.9)	33000(4.7)
$C_6H_5B(OH)_2$	48544(1.3)	46948(7.2)	45045(5.8)	44248(1.7)	39062(0.07)	38910(0.14)	38168(0.20)	37313(0.32)	36363(0.27)

Table S4. Magnetic susceptibility parameters for cobalt(II) complexes under study

Parameter	**$[Co(PzOx)_3(BC_6H_5)Cl]$**	**$[Co(FPzOx)_3(BC_6H_5)Cl]$**	**$[Co(PzOx)_3(BC_6H_5)I]$**	**$[Co(PzOx)_3(BC_6H_5)Br]$**	**$[Co(PzOx)_3(BC_6H_5)Cl] \cdot (CH_3)_2CO$**
Δ (cm^{-1})	–387	–129	–627	–521	–259
δ (cm^{-1})	–69.5	–0.12	–40.0	–33.8	–0.02
λ (cm^{-1})	–150	–119	–117	–129	–142
σ	1.38	1.53	1.58	1.55	1.63
R^2	0.97	0.85	0.99	0.85	0.99

Table S5. Parameters obtained from fit of relaxation times for the cobalt(II) complexes under study.

Parameter	**$[Co(PzOx)_3(BC_6H_5)Cl]$**	**$[Co(FPzOx)_3(BC_6H_5)Cl]$**	**$[Co(PzOx)_3(BC_6H_5)I]$**	**$[Co(PzOx)_3(BC_6H_5)Br]$**	**$[Co(PzOx)_3(BC_6H_5)Cl] \cdot (CH_3)_2CO$**
C, $s^{-1}K^{-m}$	1.56E-5	1.21E-4	1.68E-7	4.38E-5	4.13E-7
m	5.85	5.66	6.92	6.11	7.04
U, K	214.9	219.0	156.8	212.6	219.8
τ_0, s^{-1}	7.91E-9	1.5E-9	2.04E-7	2.14E-9	8.80E-9
B_1, s^{-1}	77.66	0.44	75.83	132.12	68.81
B_2, T^{-2}	1.46E5	0.1	0.0	1.41E2	9.30E3
A, $s^{-1}K^{-1}T^{-n}$	-	-	2.78E4	1.00E3	-
n	-	-	4.0	4.0	-

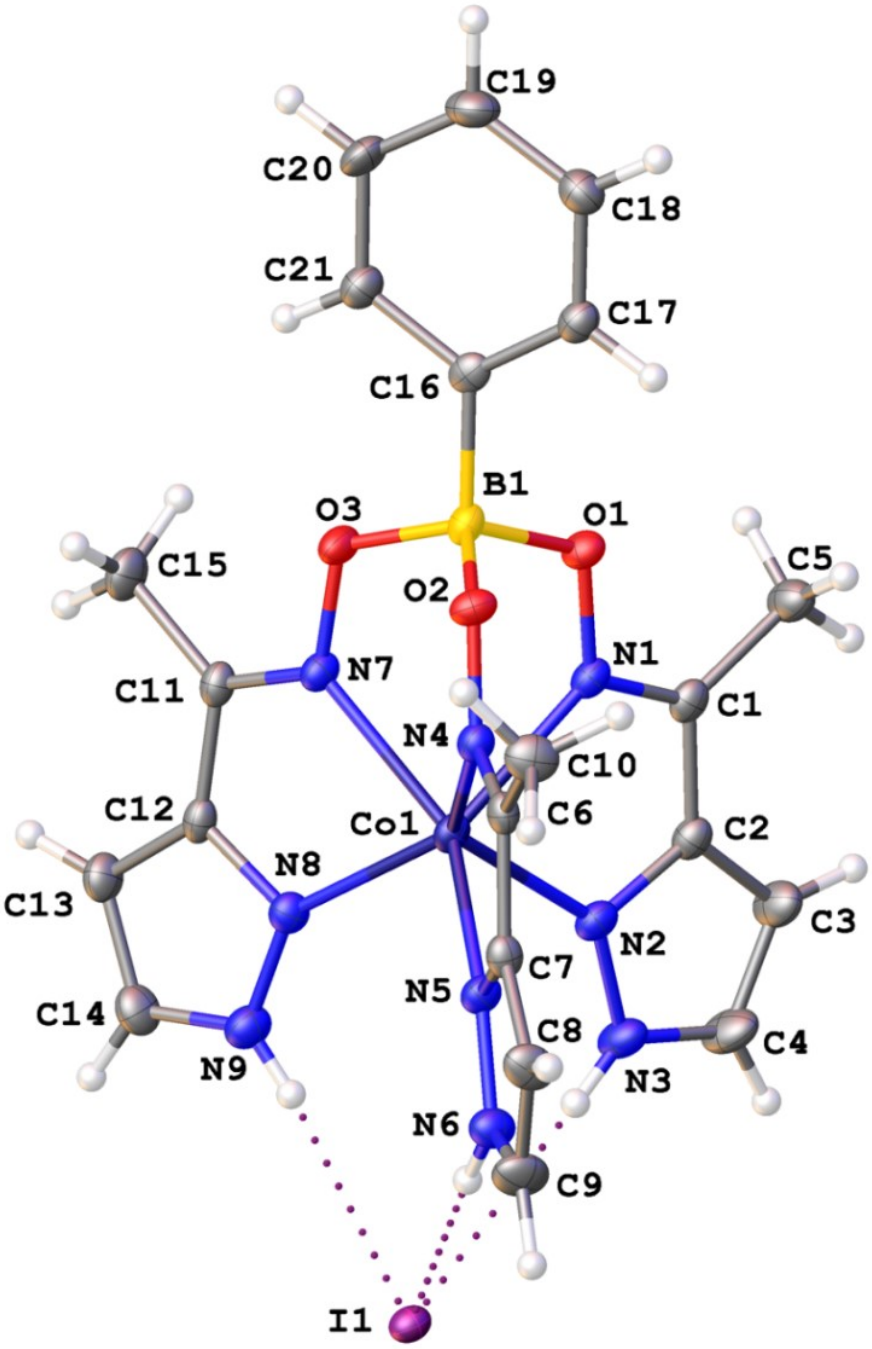

Figure S1. General view of the pseudoclathrochelate $[Co(PzOx)_3(BC_6H_5)I]$ in the mixed crystal $\{[Co(PzOx)_3(BC_6H_5)I]_{0.69}[Co(PzOx)_3(BC_6H_5)Cl]_{0.31}\}\cdot C_6H_6$; the solvent molecule of benzene and an admixture of the complex $[Co(PzOx)_3(BC_6H_5)Cl]$ are omitted for clarity. Hereinafter, non-hydrogen atoms are shown as thermal ellipsoids at 40% probability level; the hydrogen bonds are depicted with dotted lines.

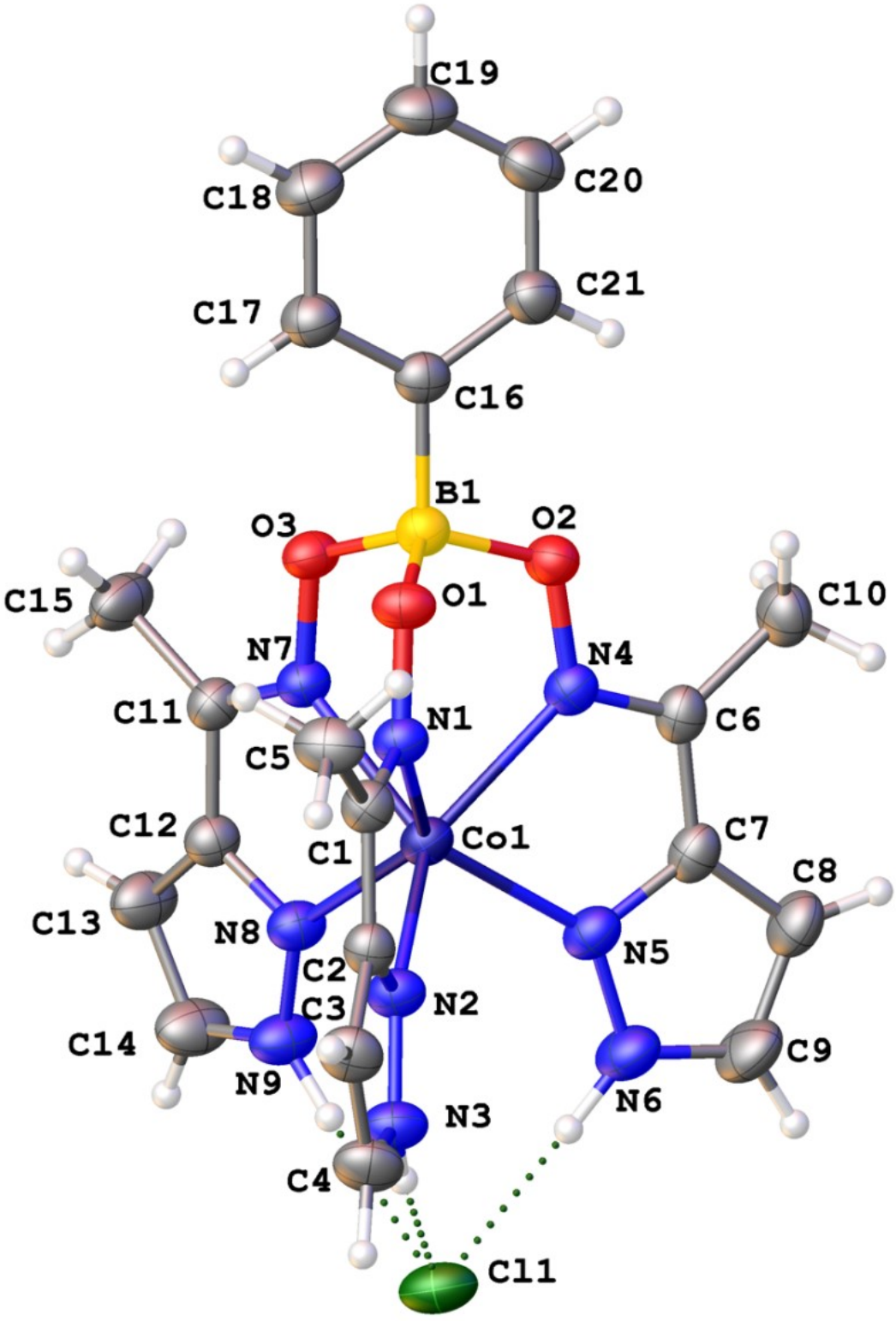

Figure S2. General view of the pseudoclathrochelate $[Co(PzOx)_3(BC_6H_5)Cl]$ in its benzene-containing solvatomorph; the disordered molecule of this solvent is omitted for clarity.

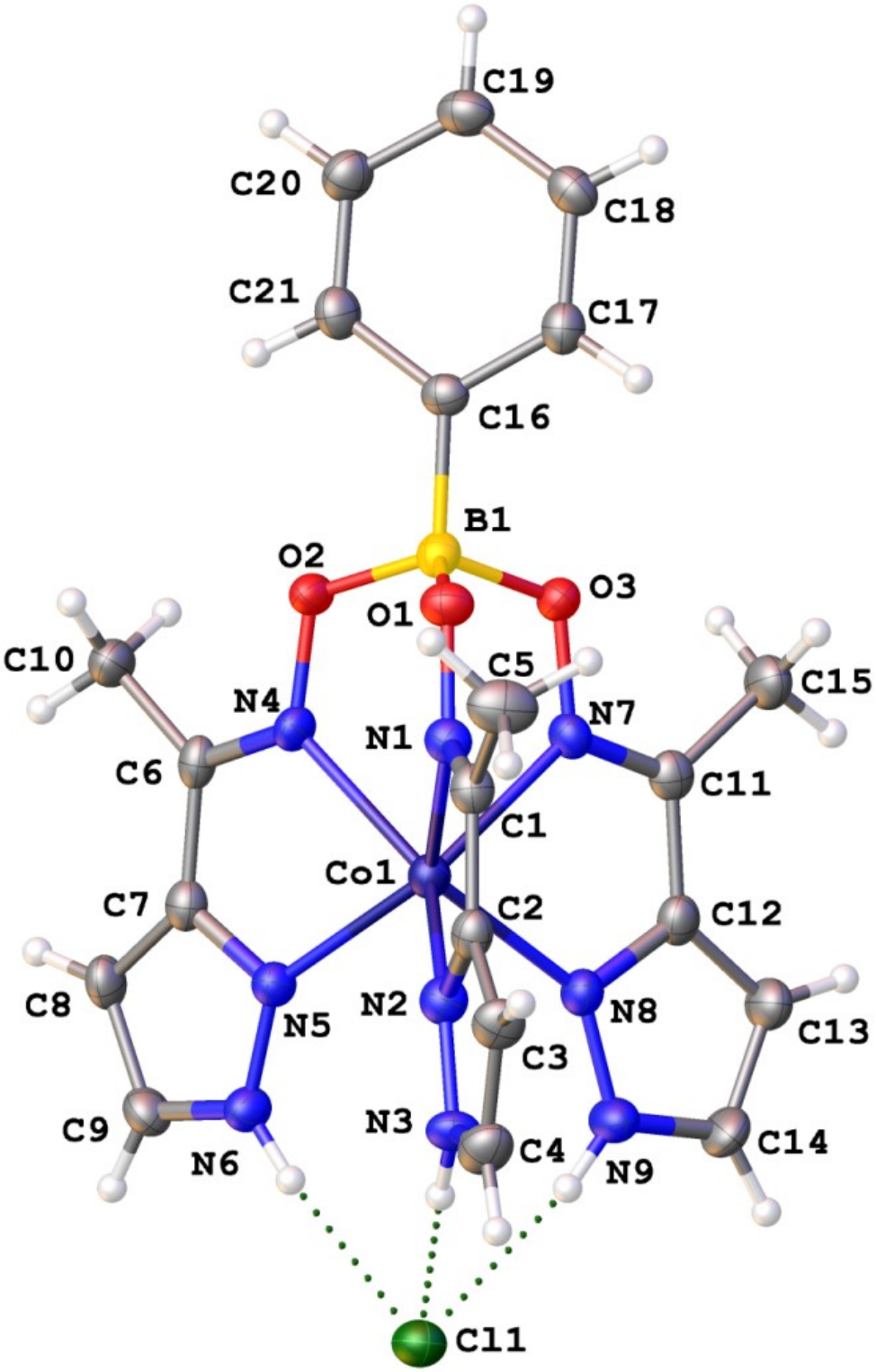

Figure S3. General view of the pseudoclathrochelate $[Co(PzOx)_3(BC_6H_5)Cl]$ in its chloroform-containing solvatomorph; the molecule of this solvent is omitted for clarity. XRD structure of this solvatomorph was reported in [S13].

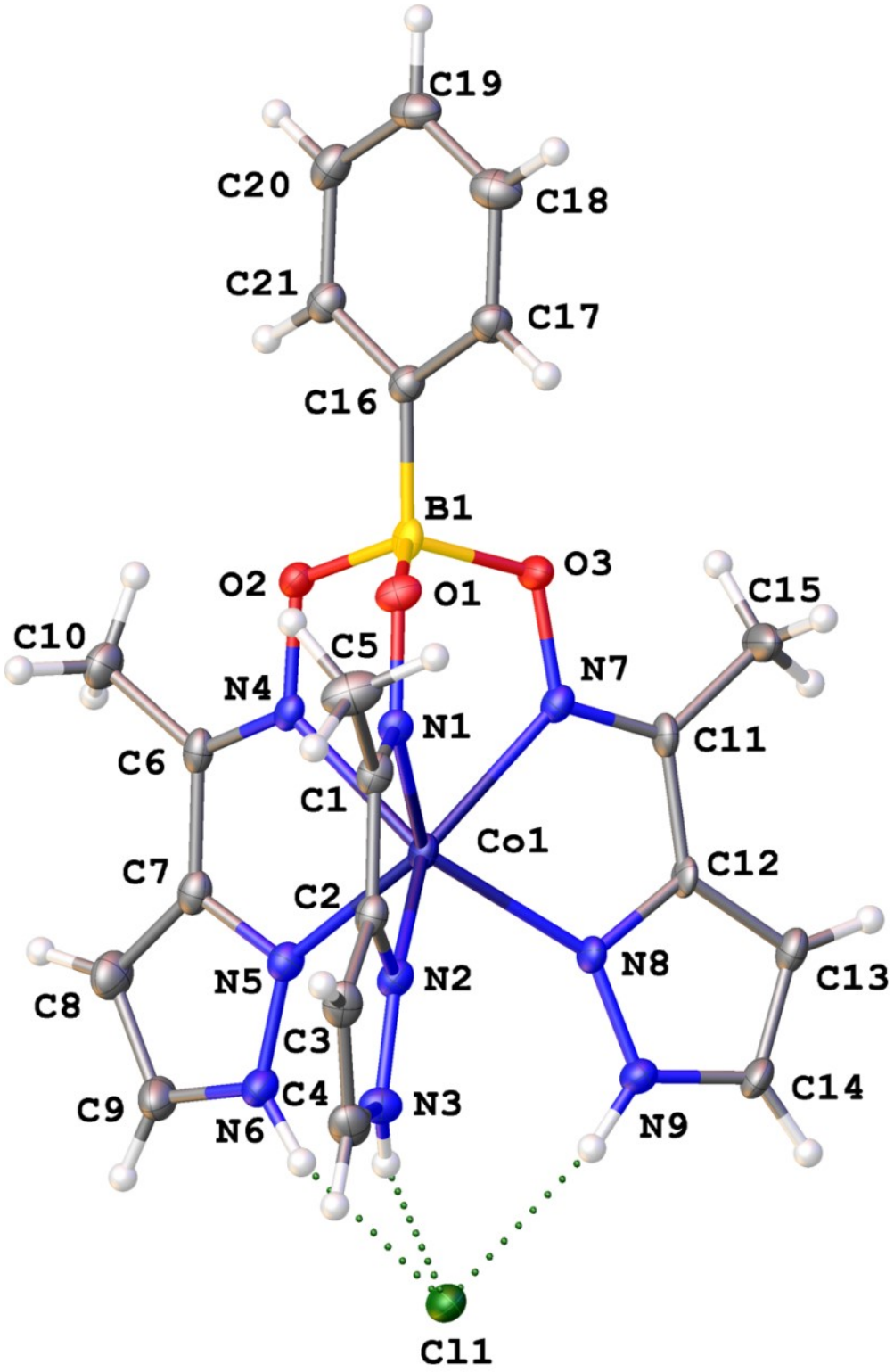

Figure S4. General view of the pseudoclathrochelate $[Co(PzOx)_3(BC_6H_5)Cl]$ in its acetone-containing solvatomorph; the molecule of this solvent is omitted for clarity.

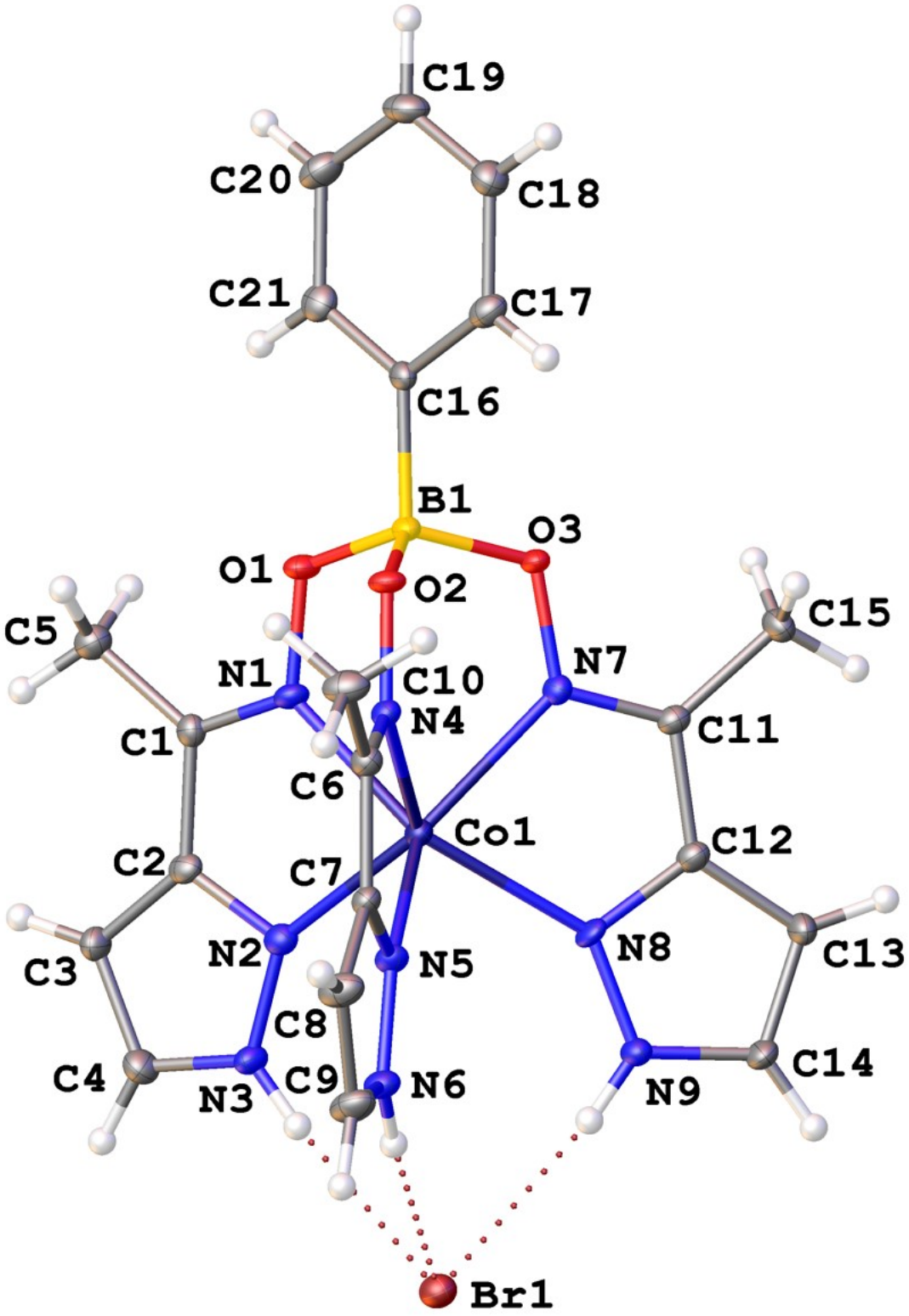

Figure S5. General view of the pseudoclathrochelate $[Co(PzOx)_3(BC_6H_5)Br]$ in its benzene-containing solvatomorph; the disordered molecule of this solvent is omitted for clarity.

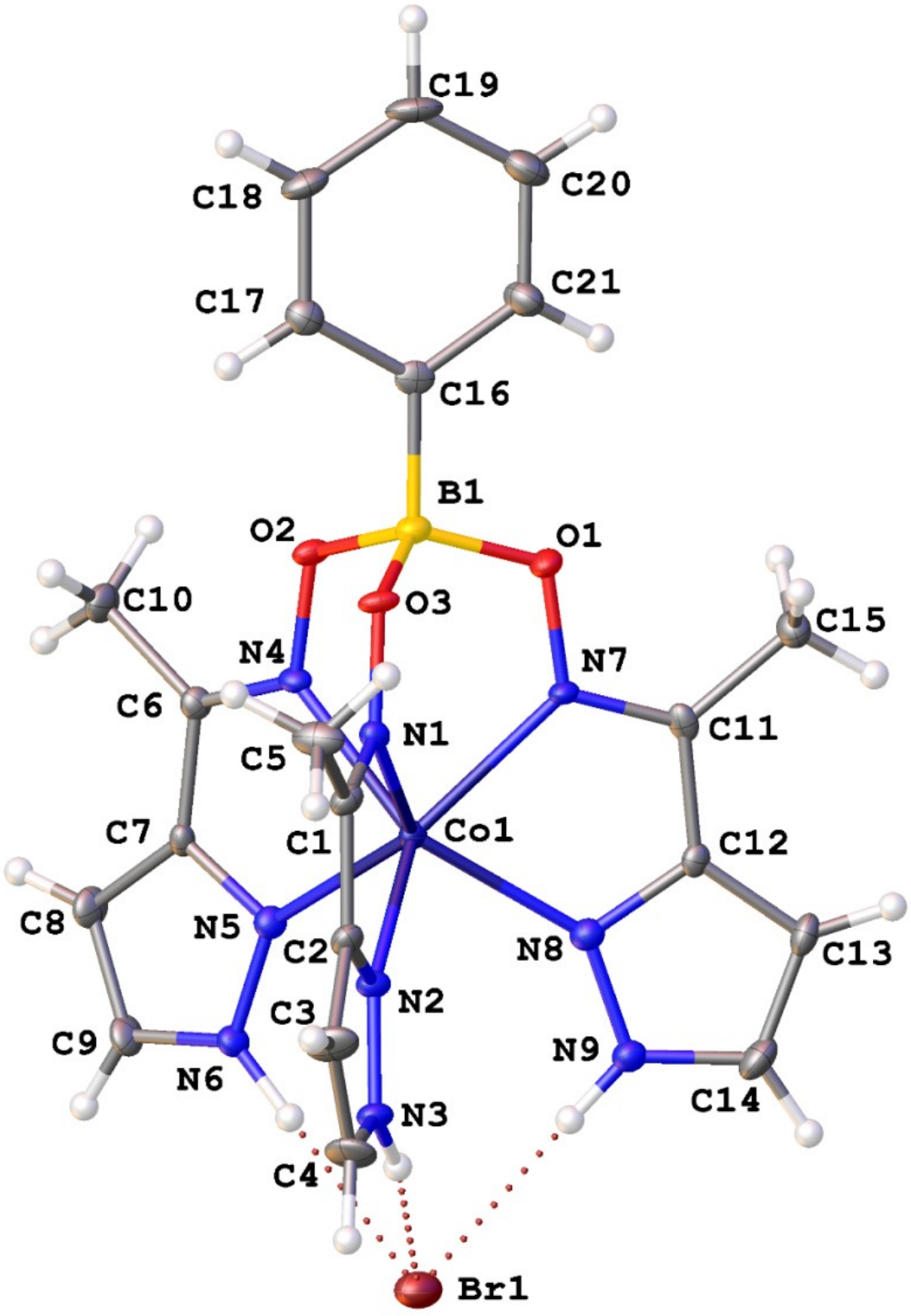

Figure S6. General view of the pseudoclathrochelate $[Co(PzOx)_3(BC_6H_5)Br]$ in its THF-containing solvatomorph; the disordered molecule of this solvent is omitted for clarity.

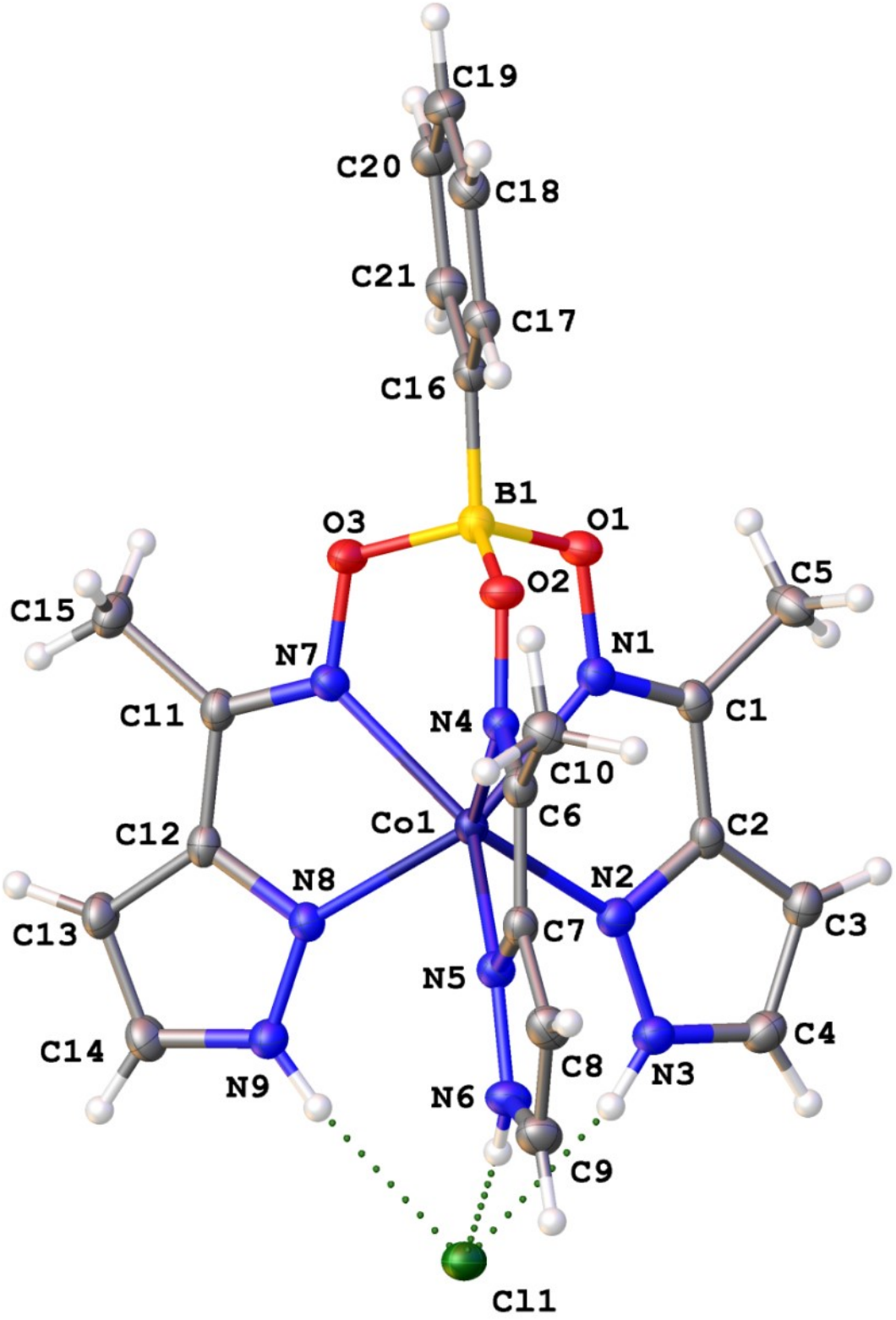

Figure S7. General view of the pseudoclathrochelate $[Co(PzOx)_3(BC_6H_5)Cl]$ in its solvent-free crystal.

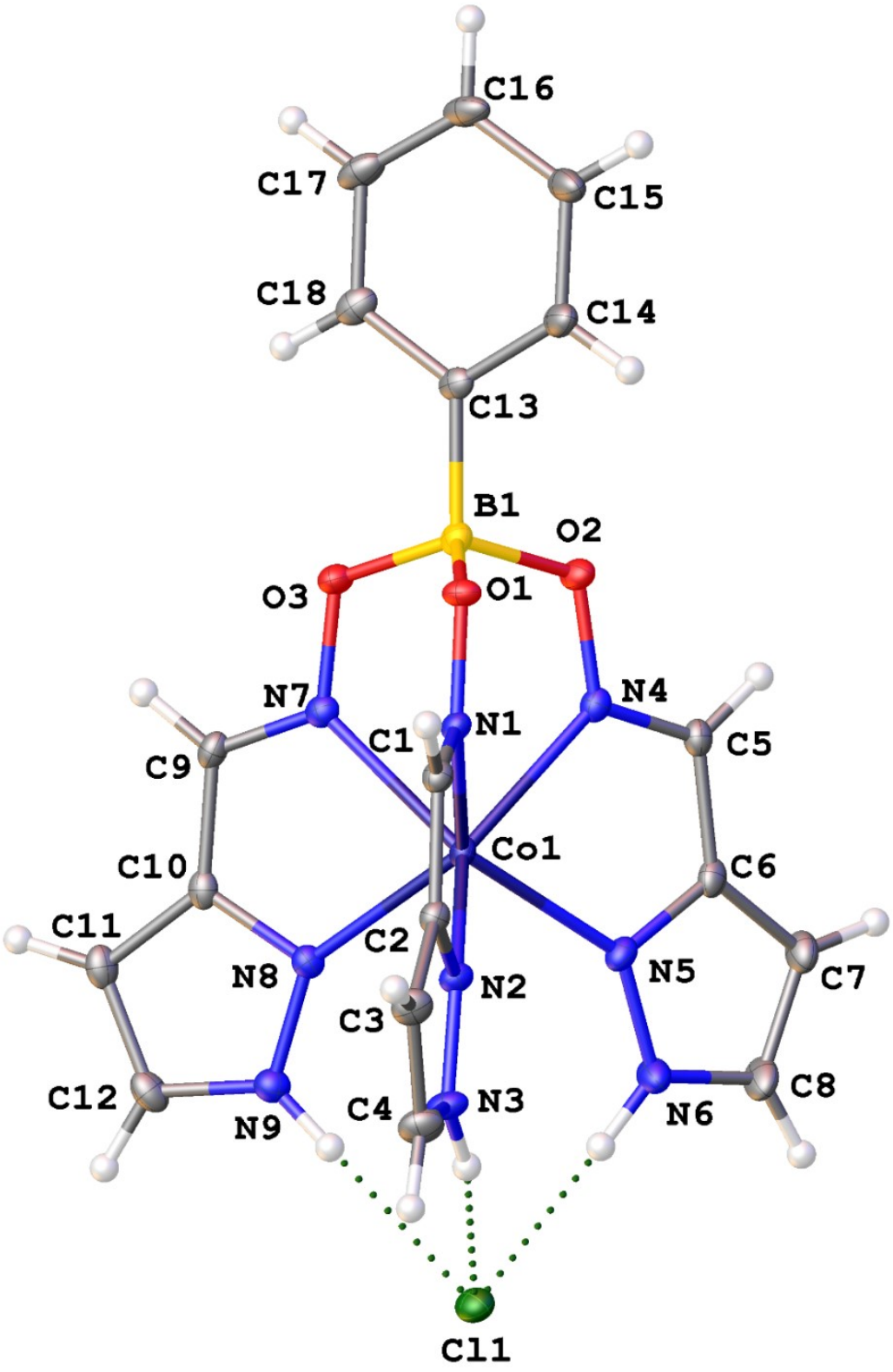

Figure S8. General view of the pseudoclathrochelate $[Co(FPzOx)_3(BC_6H_5)Cl]$ in its solvent-free crystal.

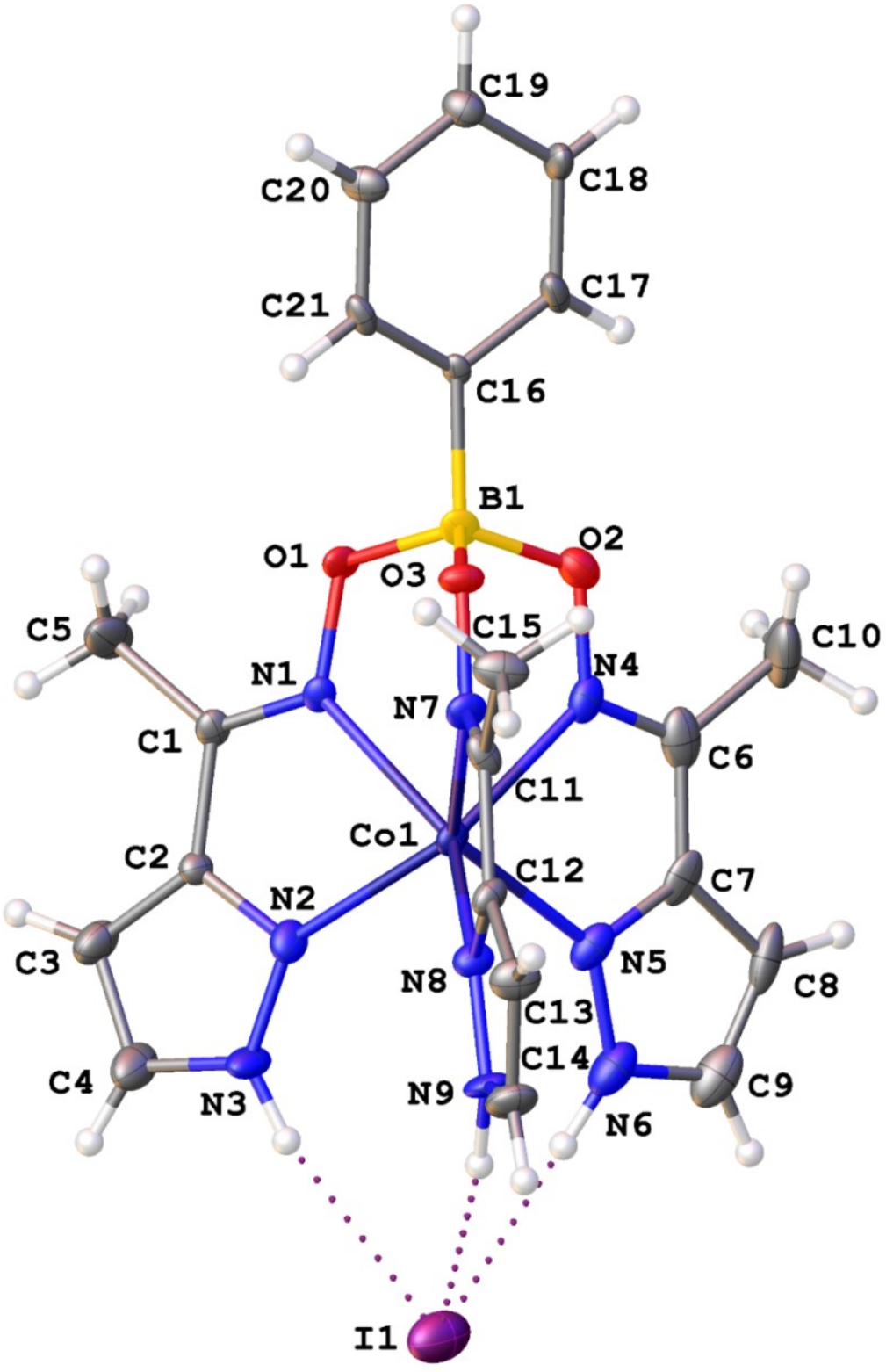

Figure S9. General view of the pseudoclathrochelate $[Co(PzOx)_3(BC_6H_5)I]$ in its solvent-free crystal; the minor component of its disordered apical phenyl substituent is omitted for clarity.

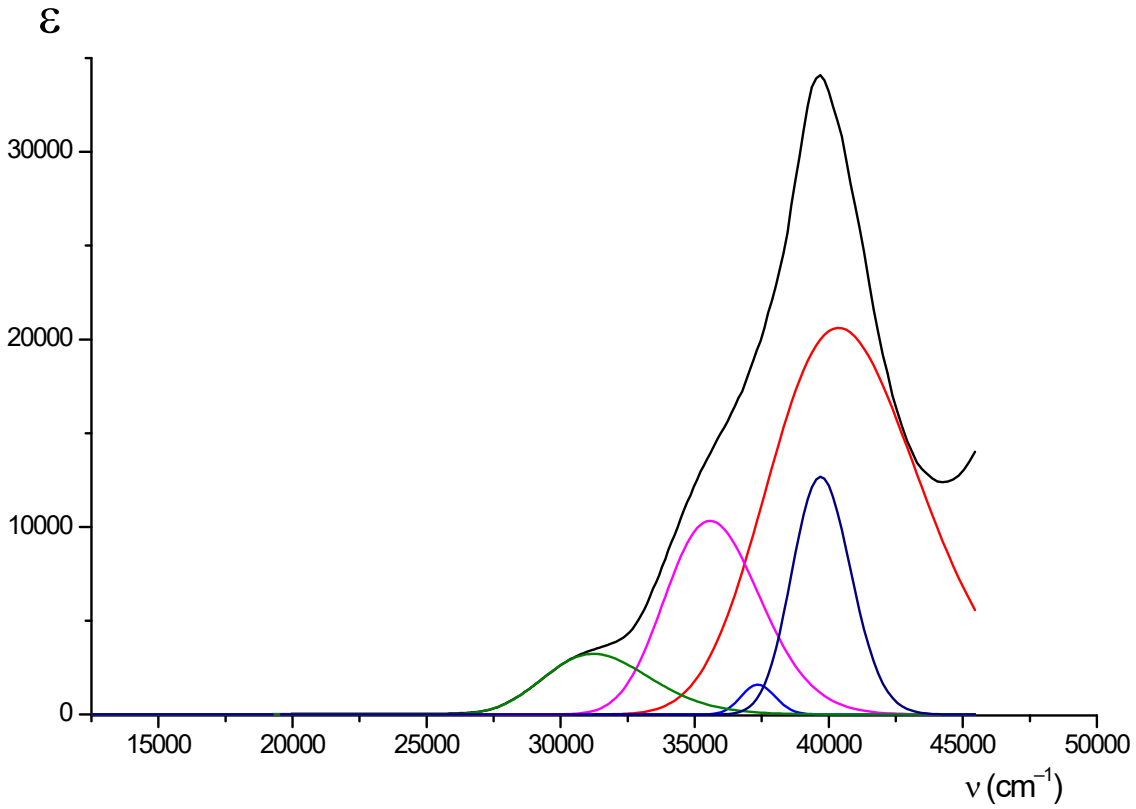

Figure S10. Solution UV-vis spectrum of the pseudoclathrochelate $[Co(FPzOx)_3(BC_6H_5)Cl]$ in acetonitrile (shown in black line) and its deconvolution into the Gaussian components (shown in color lines)

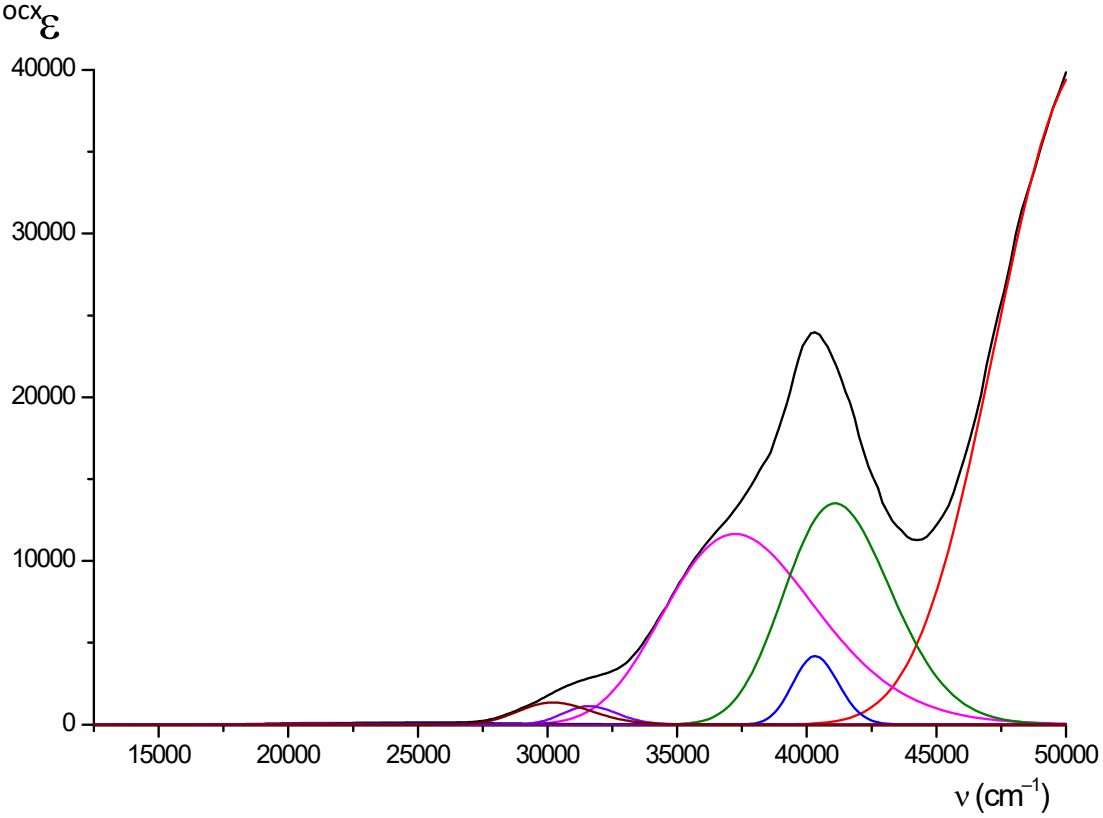

Figure S11. Solution UV-vis spectrum of the pseudoclathrochelate $[Co(PzOx)_3(BC_6H_5)Cl]$ in acetonitrile (shown in black line) and its deconvolution into the Gaussian components (shown in color lines)

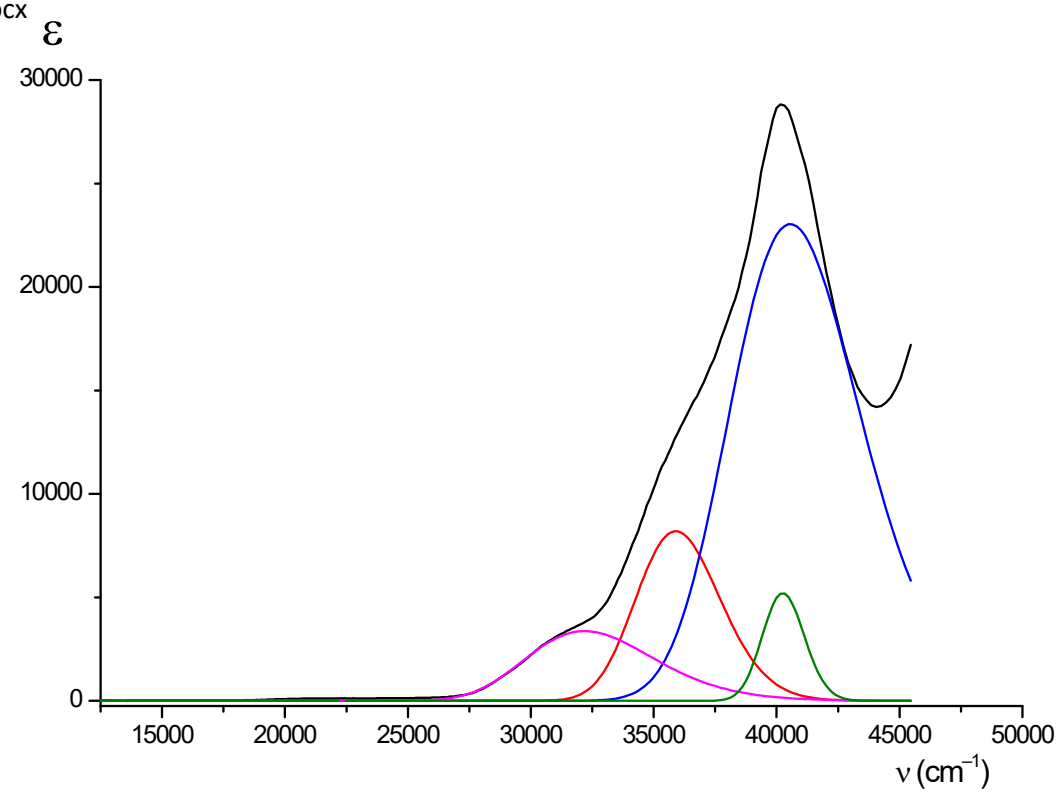

Figure S12. Solution UV-vis spectrum of the pseudoclathrochelate $[Co(PzOx)_3(BC_6H_5)Br]$ in acetonitrile (shown in black line) and its deconvolution into the Gaussian components (shown in color lines)

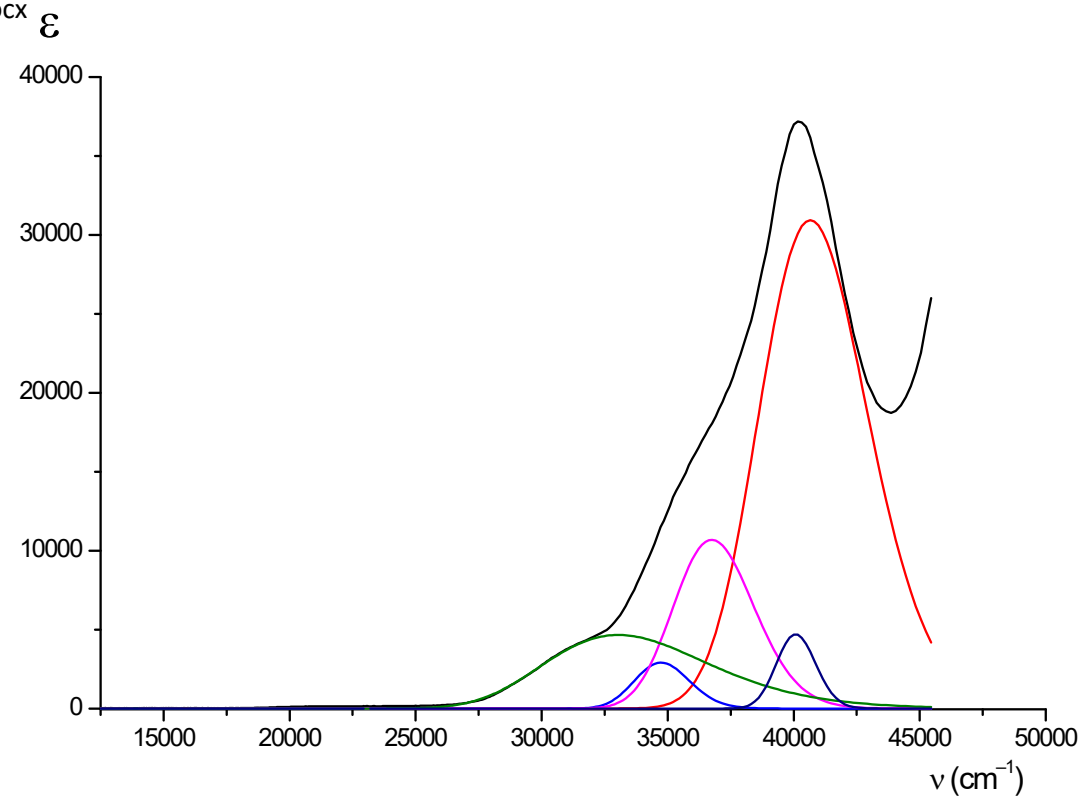

Figure S13. Solution UV-vis spectrum of the pseudoclathrochelate $[Co(PzOx)_3(BC_6H_5)I]$ in acetonitrile (shown in black line) and its deconvolution into the Gaussian components (shown in color lines)

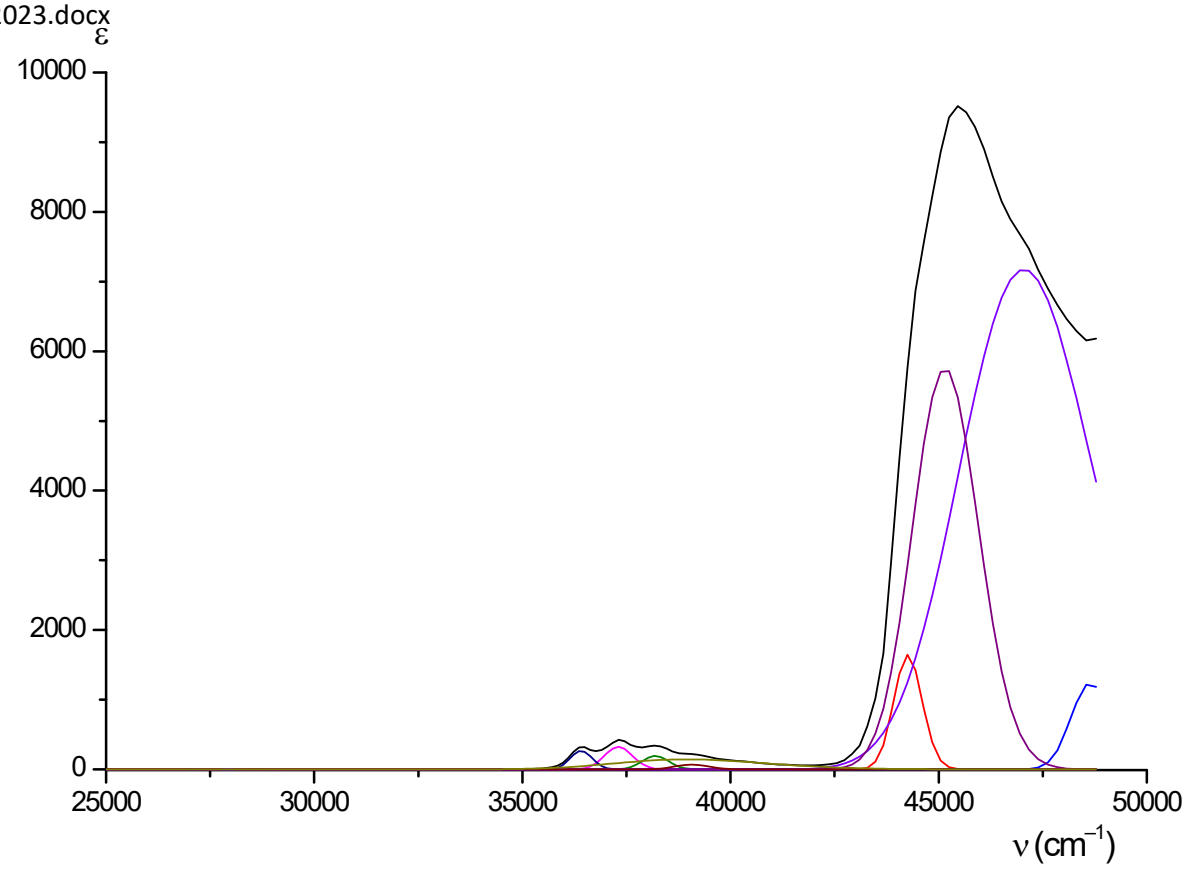

Figure S14. Solution UV-vis spectrum of the phenylboronic acid as a cross-linking ligand synthon in ethanol (shown in black line) and its deconvolution into the Gaussian components (shown in color lines).

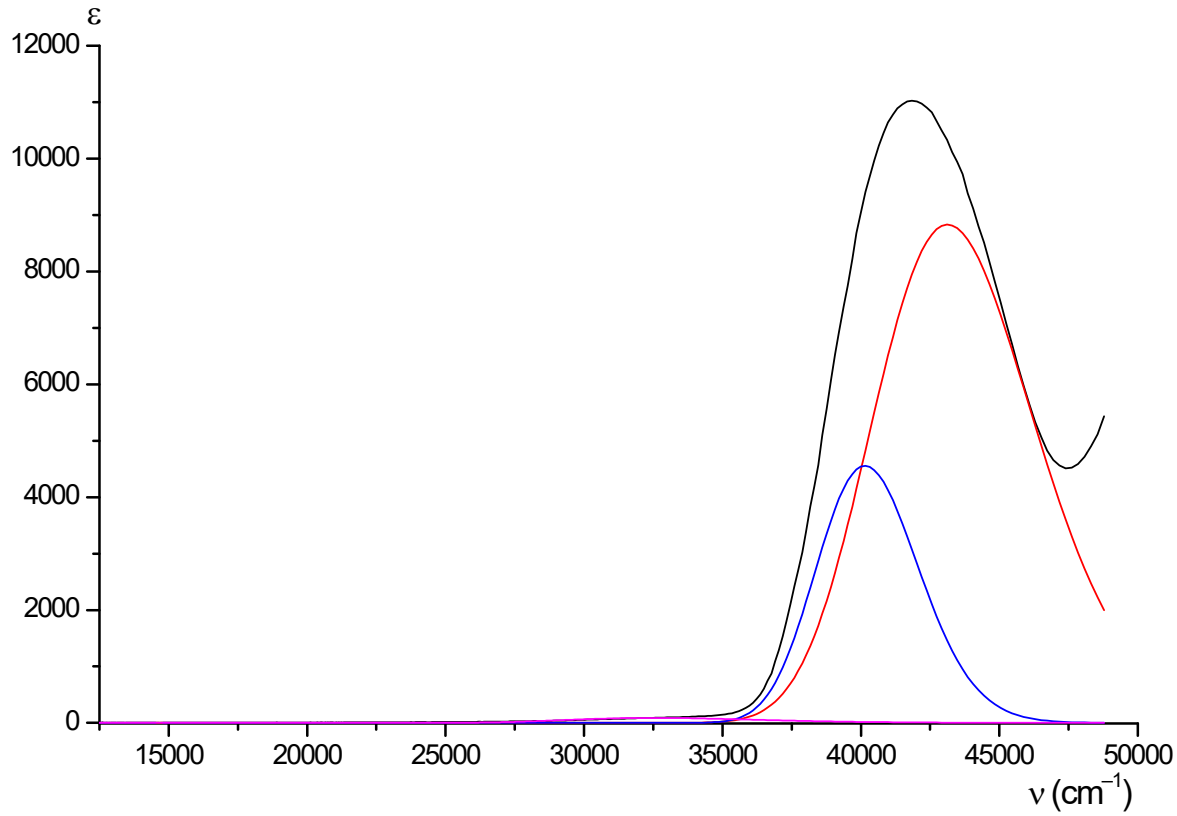

Figure S15. Solution UV-vis spectrum of the pseudoclathrochelate *PzOxH* as a chelating ligand synthon in ethanol (shown in black line) and its deconvolution into the Gaussian components (shown in color lines).

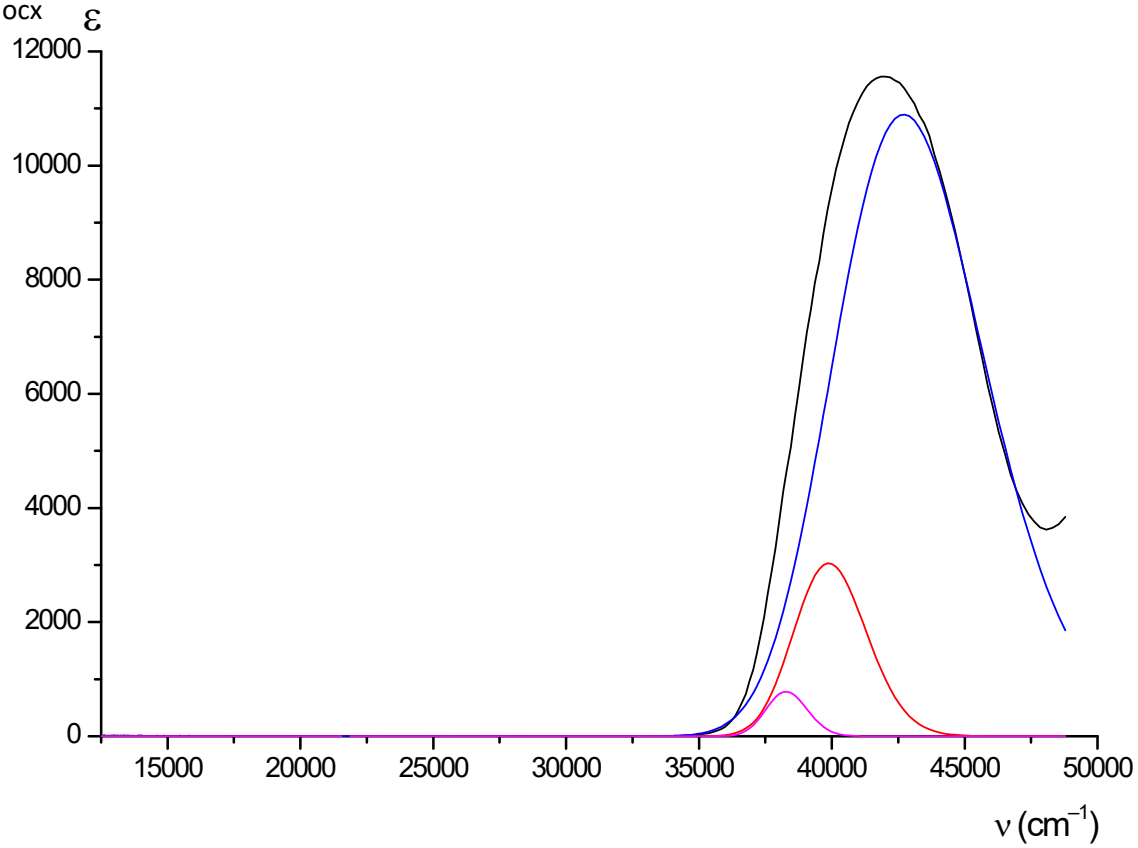

Figure S16. Solution UV-vis spectrum of the pseudoclathrochelate *FPzOxH* as a chelating ligand synthon in ethanol (shown in black line) and its deconvolution into the Gaussian components (shown in color lines)

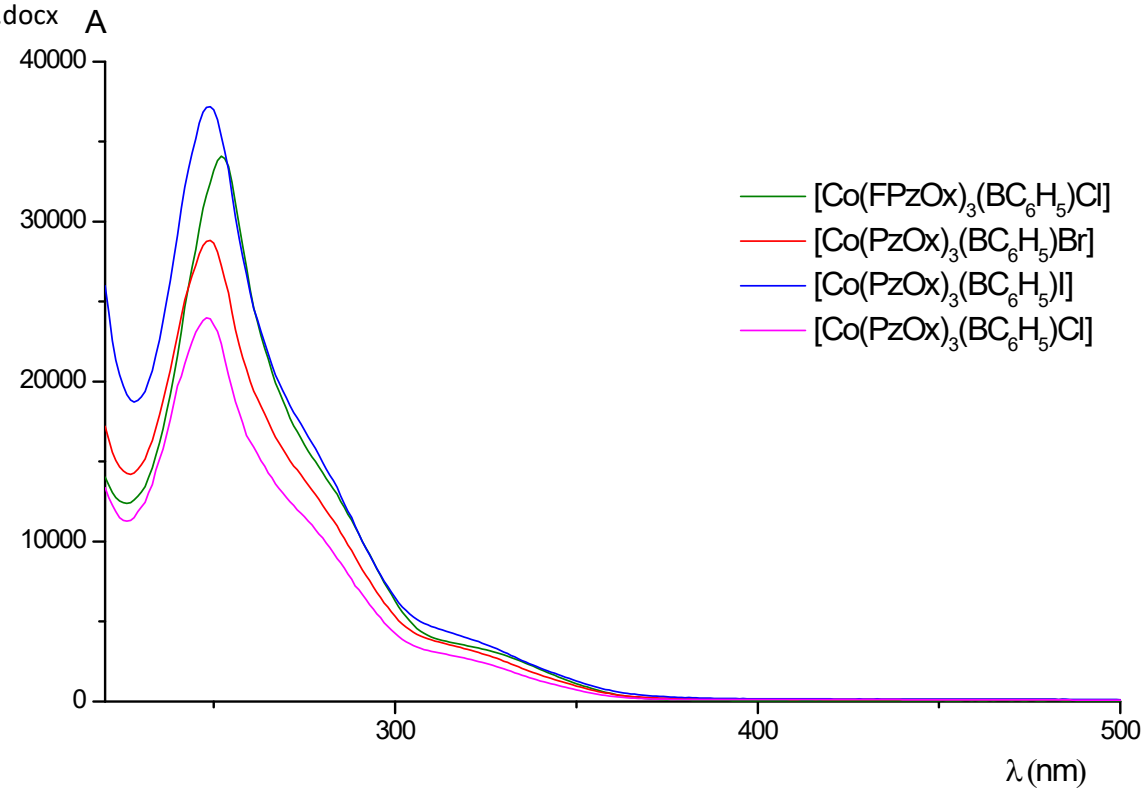

Figure S17. Solution UV-vis spectra of the obtained cobalt(II) pseudoclathrochelates in acetonitrile.

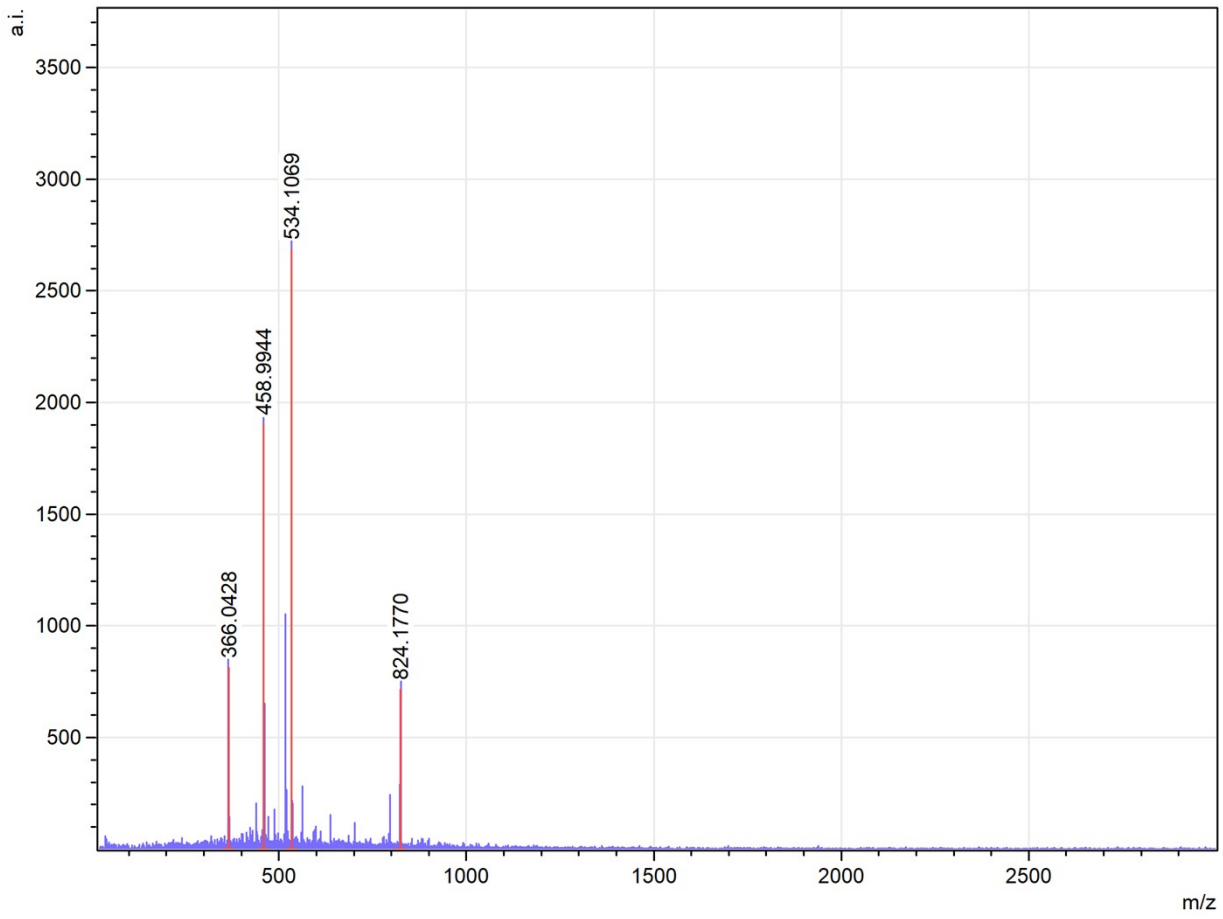

Figure S18. Mass-spectrum of the complex $[Co(FPzOx)_3(BC_6H_5)Cl]$.

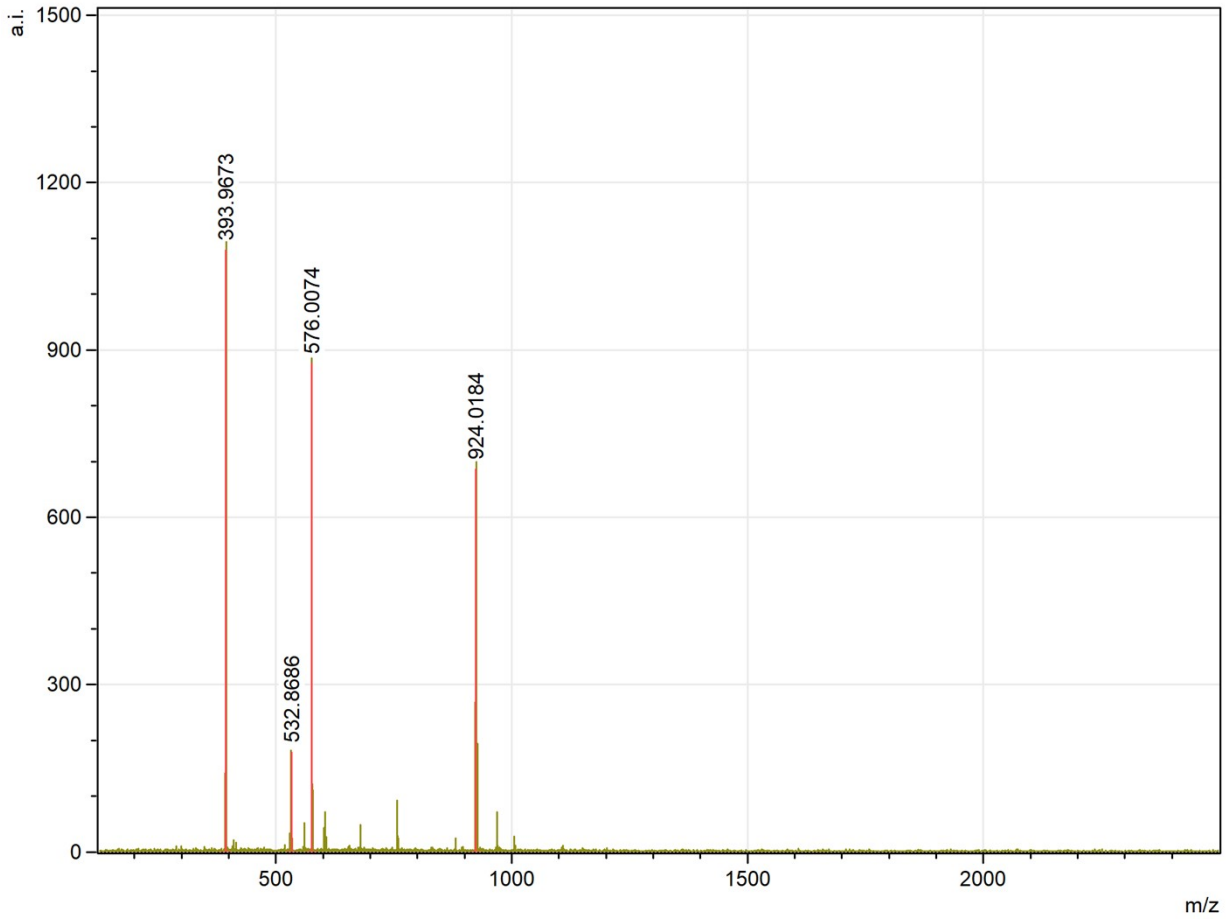

Figure S19. Mass-spectrum of the complex $[Co(PzOx)_3(BC_6H_5)Br]$.

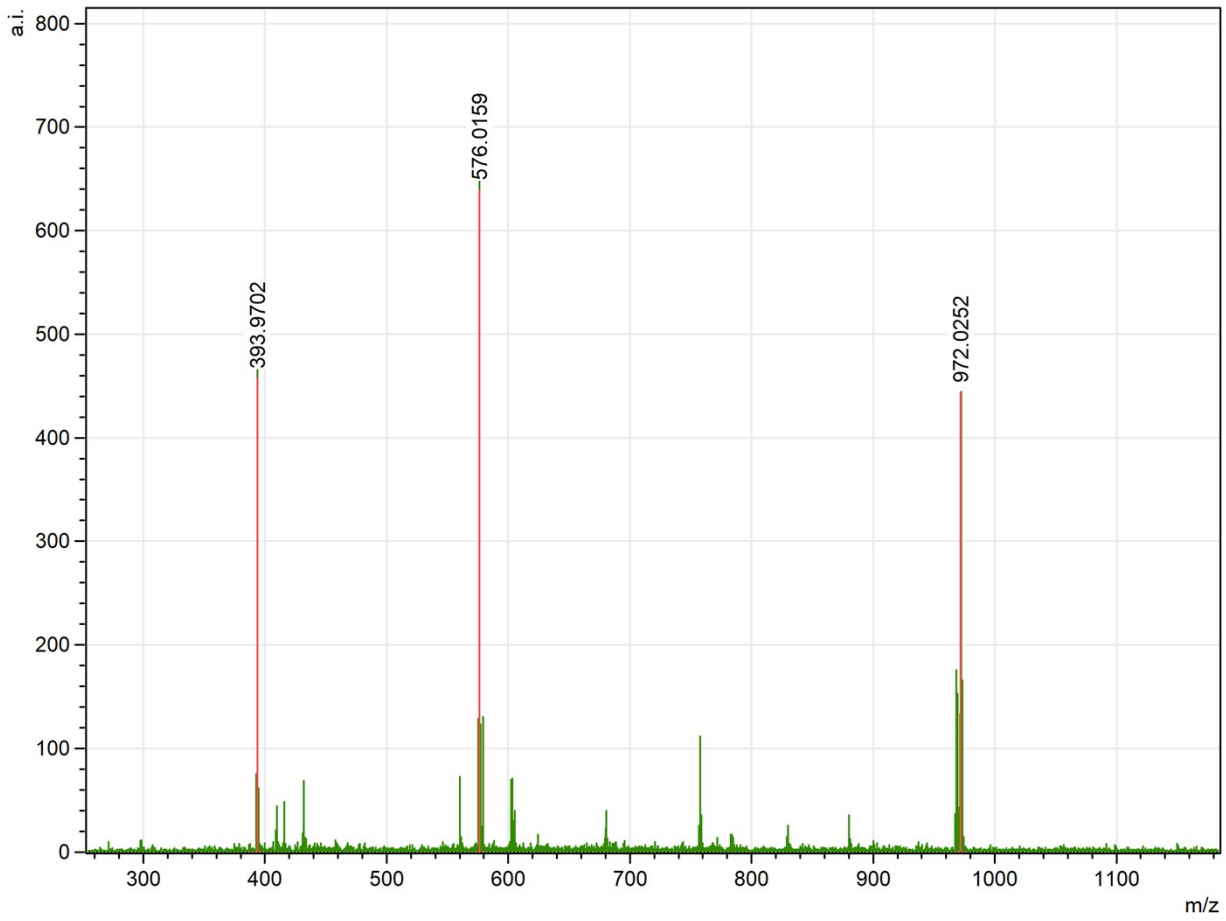

Figure S20. Mass-spectrum of the complex $[Co(PzOx)_3(BC_6H_5)I]$.

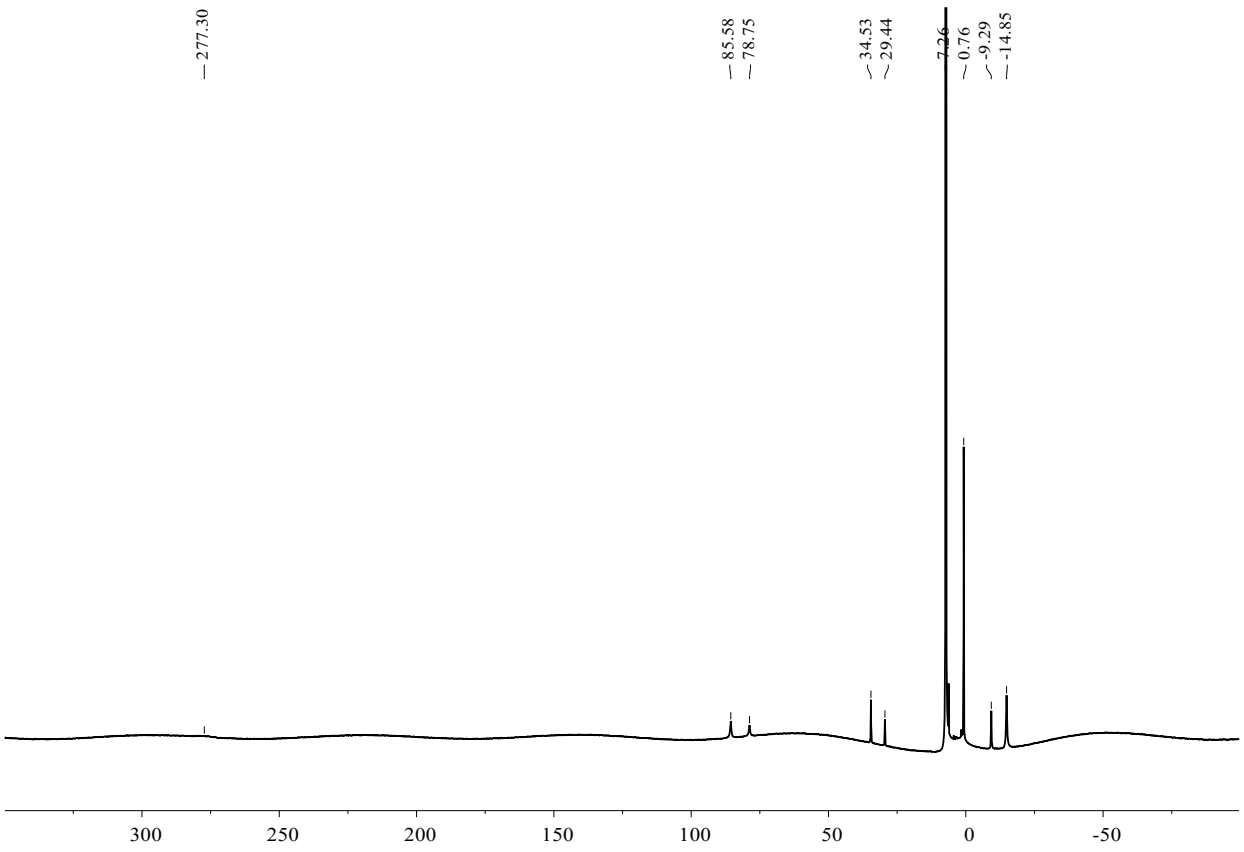

Figure S21. Solution ^{1}H NMR spectrum of the complex $[Co(PzOx)_3(BC_6H_5)Cl]$ in $CDCl_3$.

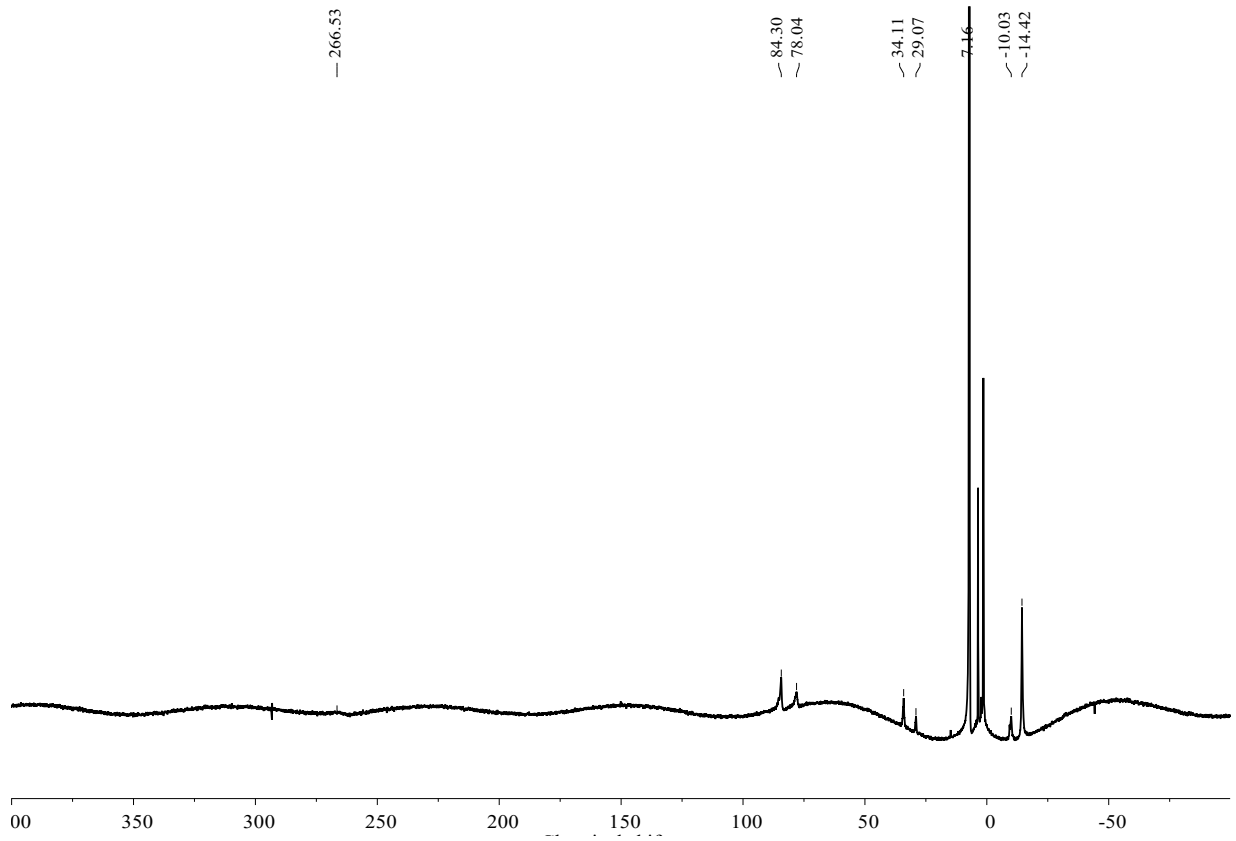

Figure S22. Solution ^{1}H NMR spectrum of the complex $[Co(PzOx)_3(BC_6H_5)I]$ in C_6D_6.

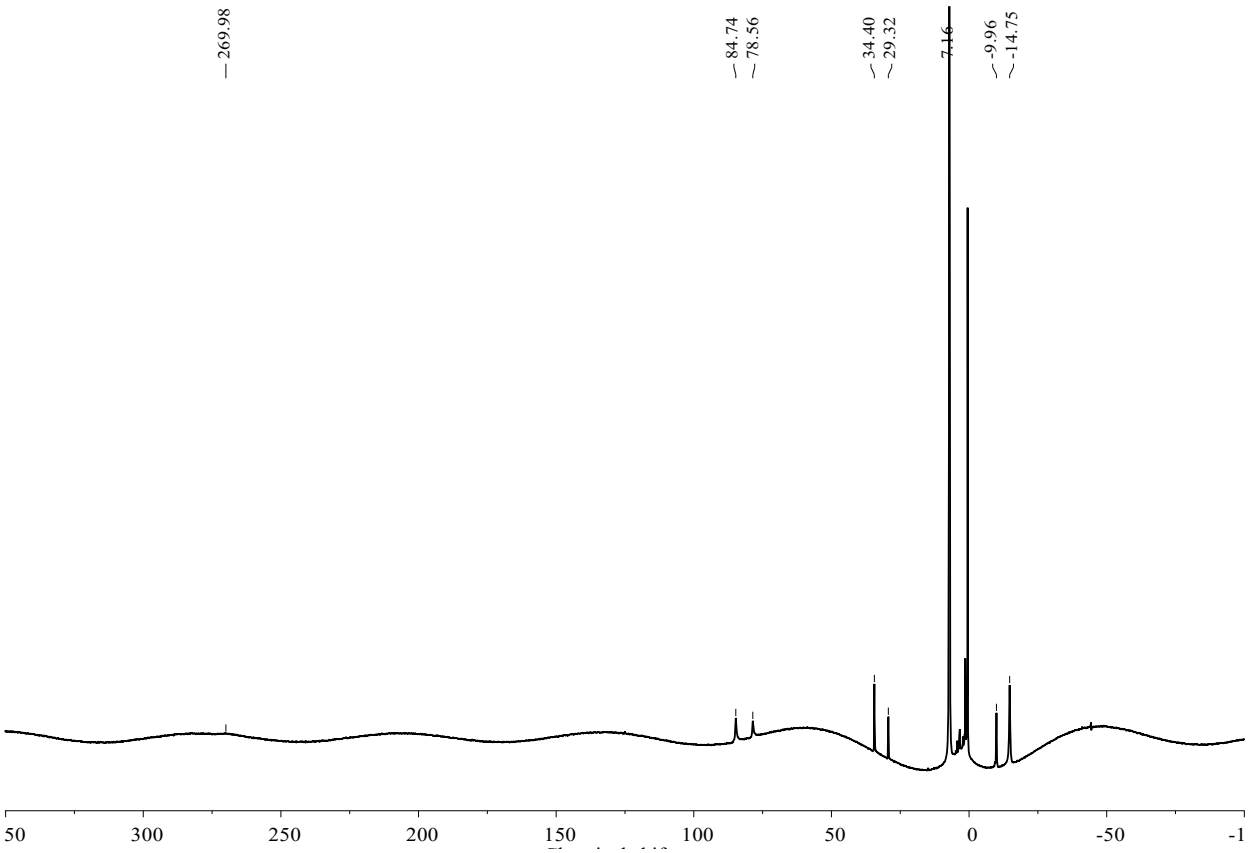

Figure S23. Solution ^{1}H NMR spectrum of the complex $[Co(PzOx)_3(BC_6H_5)Br]$ in C_6D_6.

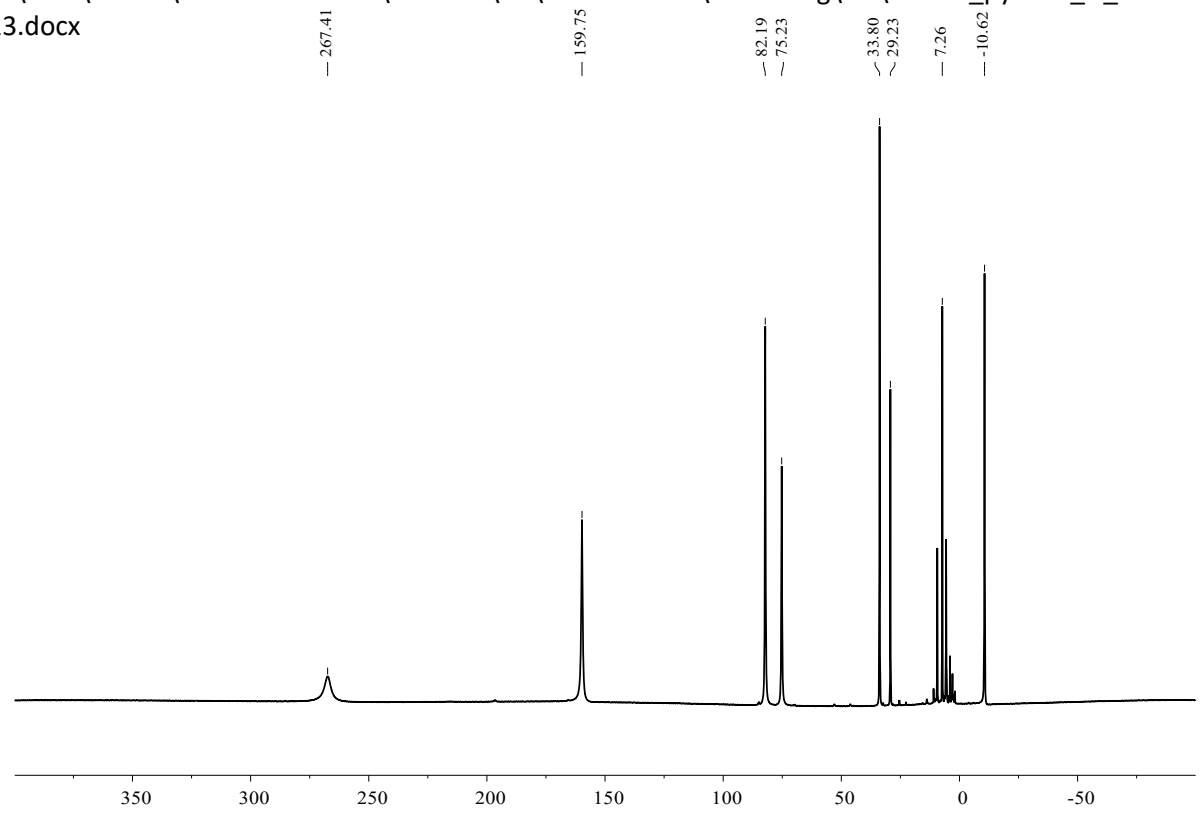

Figure S24. Solution ^{1}H NMR spectrum of the complex $[Co(FPzOx)_3(BC_6H_5)Cl]$ in $CDCl_3$.

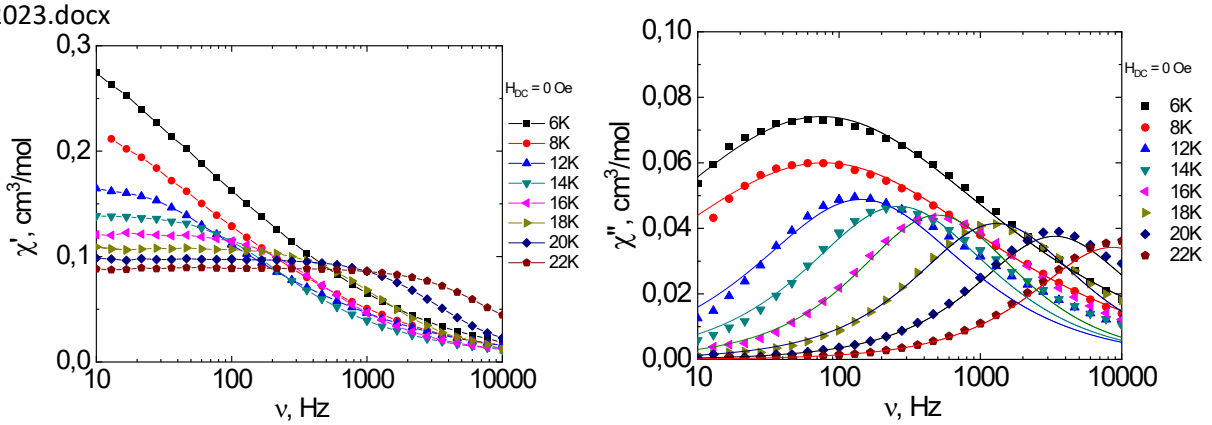

Figure S25. In-phase (χ') and out-of-phase (χ'') ac magnetic susceptibility for $[Co(PzOx)_3(BC_6H_5)Cl]$ at zero dc magnetic field measured at various temperatures. The solid lines for out-of-phase χ'' magnetic susceptibility display approximation by the generalized Debye model.

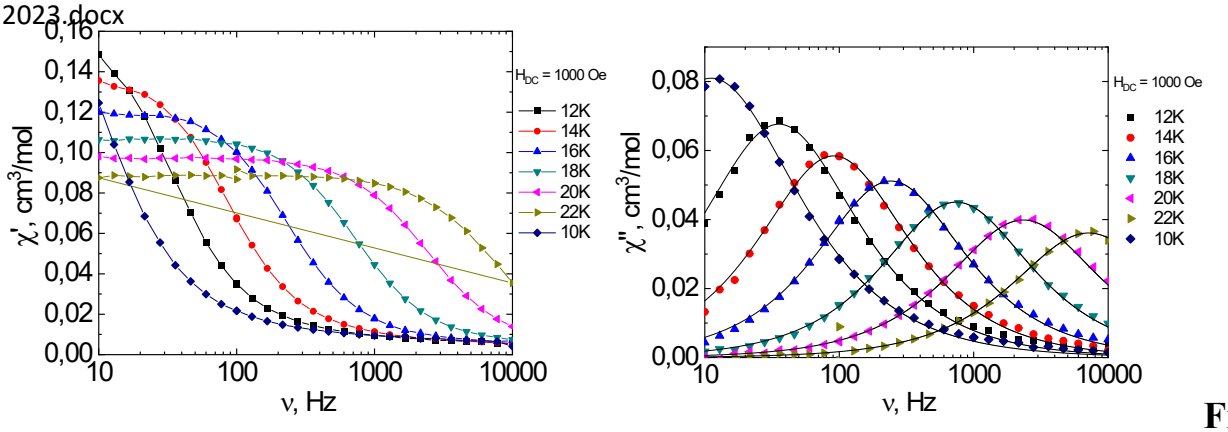

Figure S26. In-phase (χ') and out-of-phase (χ'') ac magnetic susceptibility for $[Co(PzOx)_3(BC_6H_5)Cl]$ at zero dc magnetic field measured at various temperatures. The solid lines for out-of-phase χ'' magnetic susceptibility display approximation by the generalized Debye model.

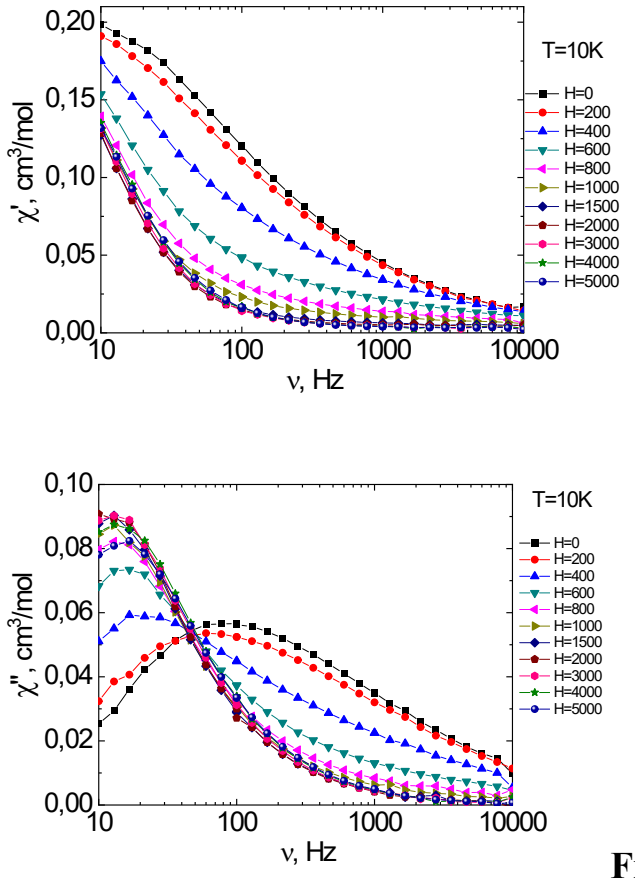

Figure S27. In-phase (χ') and out-of-phase (χ'') ac magnetic susceptibility for $[Co(PzOx)_3(BC_6H_5)Cl]$ measured at varied dc magnetic field at 10 K. The solid lines for out-of-phase χ'' magnetic susceptibility display approximation by the generalized Debye model.

Table S6. Relaxation times for the complex $[Co(PzOx)_3(BC_6H_5)Cl]$ in zero and 1000 Oe dc field.

T K	τ, s (H = 0 Oe)	τ, s (H = 1000 Oe)
6	0.01323	n/d
8	0.01282	n/d
10	n/d	0.089565
12	0.00709	0.02815
14	0.00378	0.010989
16	0.002016	4.13E-03
18	7.68E-04	1.35E-03
20	2.94E-04	4.16E-04
22	1.16E-04	1.41E-04

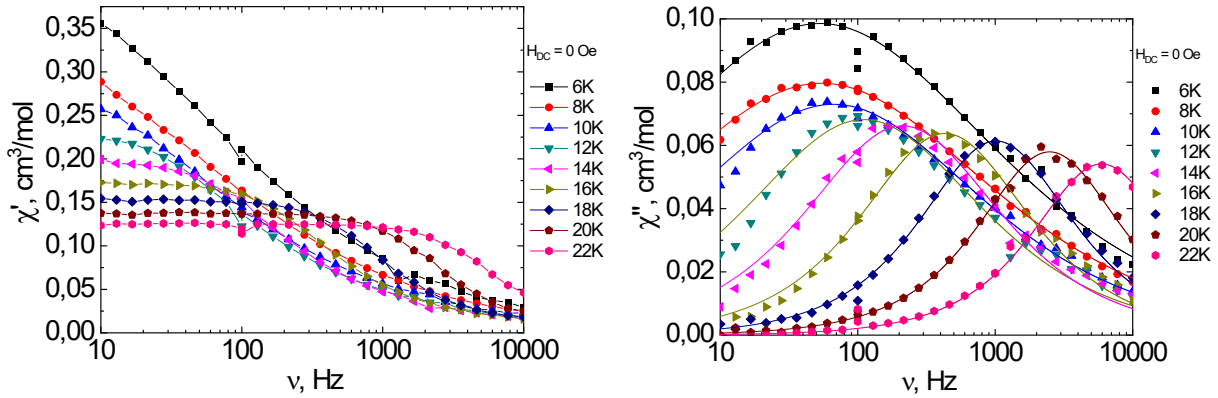

Figure S28. In-phase (χ') and out-of-phase (χ'') ac magnetic susceptibility for $[Co(PzOx)_3(BC_6H_5)Cl] \cdot (CH_3)_2CO$ at zero DC magnetic field measured at various temperatures. The solid lines for out-of-phase χ'' magnetic susceptibility display approximation by the generalized Debye model.

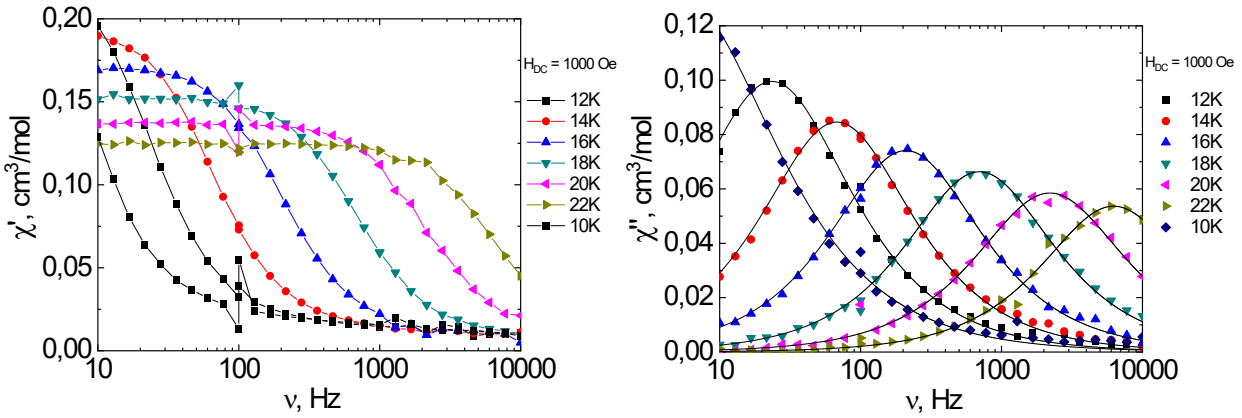

Figure S29. In-phase (χ') and out-of-phase (χ'') ac magnetic susceptibility for $[Co(PzOx)_3(BC_6H_5)Cl] \cdot (CH_3)_2CO$ measured at dc external magnetic field of 1 kOe and at various temperatures. The solid lines for out-of-phase χ'' magnetic susceptibility display approximation by the generalized Debye model.

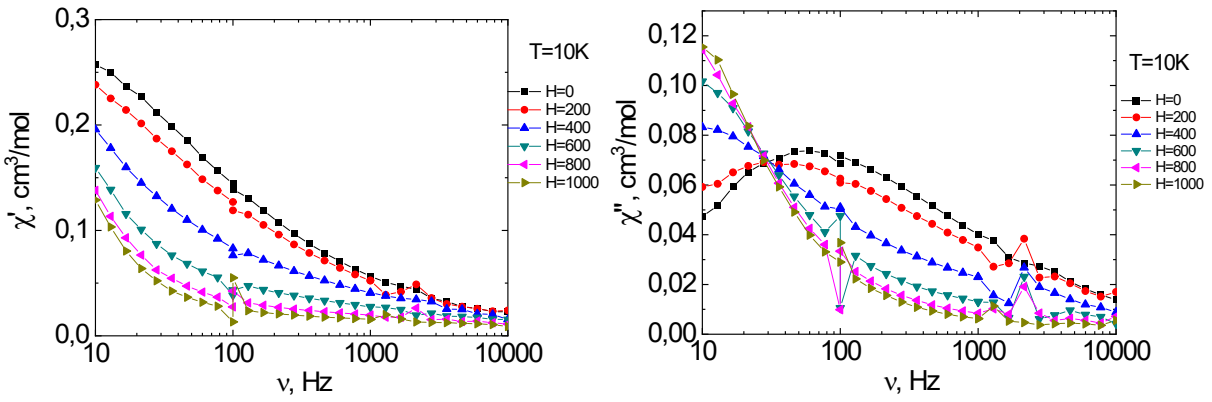

Figure S30. In-phase (χ') and out-of-phase (χ'') ac magnetic susceptibility for $[Co(PzOx)_3(BC_6H_5)Cl] \cdot (CH_3)_2CO$ measured at varied external magnetic field at 10 K. The solid lines are visual guides.

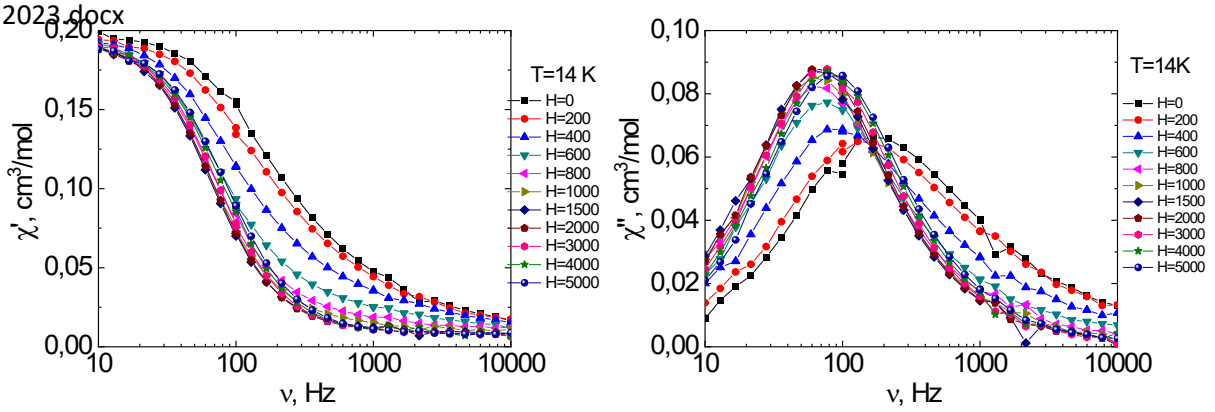

Figure S31. In-phase (χ') and out-of-phase (χ'') ac magnetic susceptibility for $[Co(PzOx)_3(BC_6H_5)Cl] \cdot (CH_3)_2CO$ measured at varied external magnetic field at 14 K. The solid lines are visual guides.

Table S7. Relaxation times for the complex $[Co(PzOx)_3(BC_6H_5)Cl] \cdot (CH_3)_2CO$ in zero and 1000 Oe dc field.

T K	τ, s (H = 0 Oe)	τ, s (H= 1000 Oe)
6	0.0188	n/d
8	0.0183	n/d
10	0.015	0.18859
12	0.0090	0.042598
14	0.00473	0.014735
16	0.002318	4.77E-03
18	0.000987	1.43E-03
20	0.000402	4.54E-04
22	0.0001688	1.60E-04

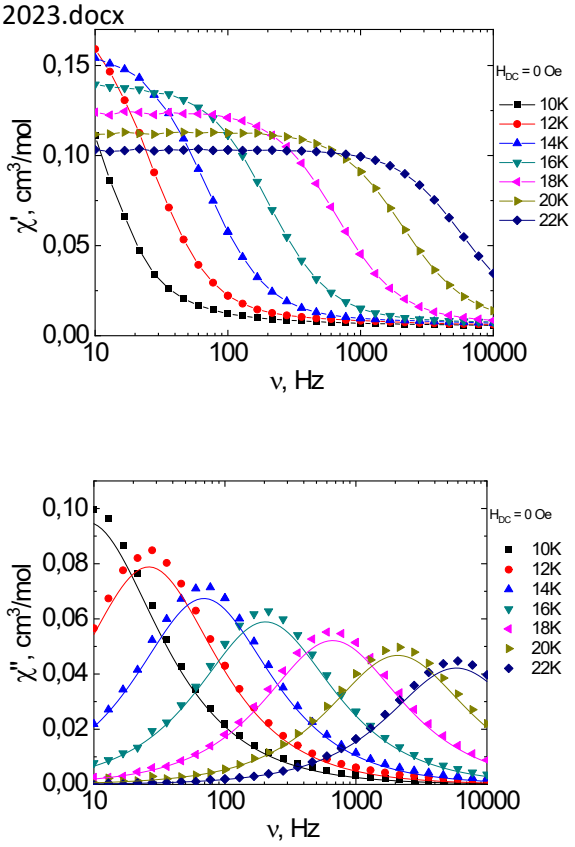

Figure S32. In-phase (χ') and out-of-phase (χ'') ac magnetic susceptibility for $[Co(FPzOx)_3(BC_6H_5)Cl]$ measured at zero dc magnetic field and at various temperatures. The solid lines for out-of-phase χ'' magnetic susceptibility display approximation by the generalized Debye model.

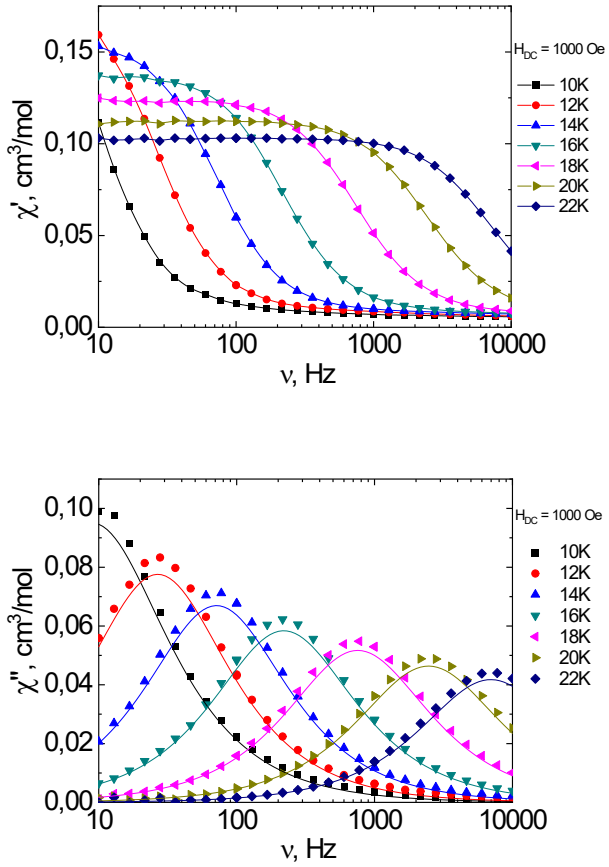

Figure S33. In-phase (χ') and out-of-phase (χ'') ac magnetic susceptibility for $[Co(FPzOx)_3(BC_6H_5)Cl]$ measured at 1000 Oe dc magnetic field and at various temperatures. The solid lines for out-of-phase χ'' magnetic susceptibility display approximation by the generalized Debye model.

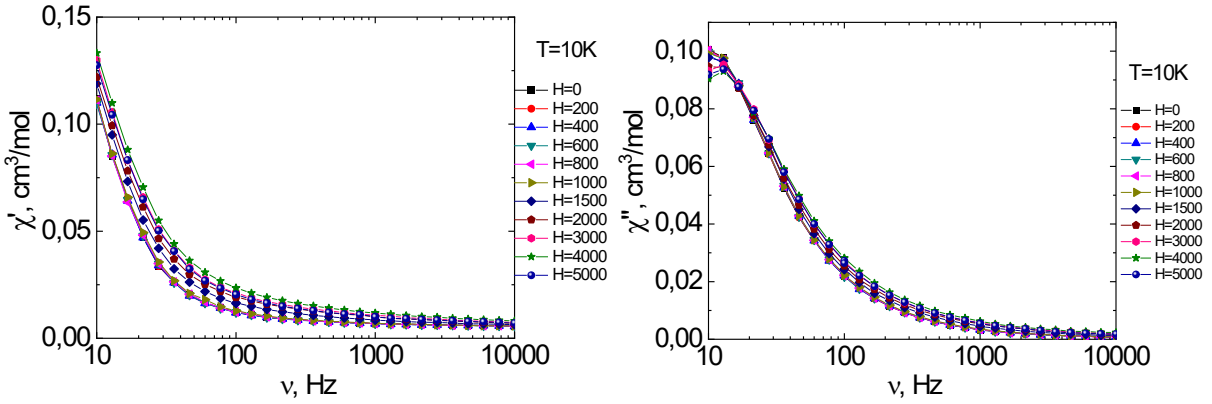

Figure S34. In-phase (χ') and out-of-phase (χ'') ac magnetic susceptibility for $[Co(FPzOx)_3(BC_6H_5)Cl]$ measured at varied external magnetic field at 10 K. The solid lines are visual guides.

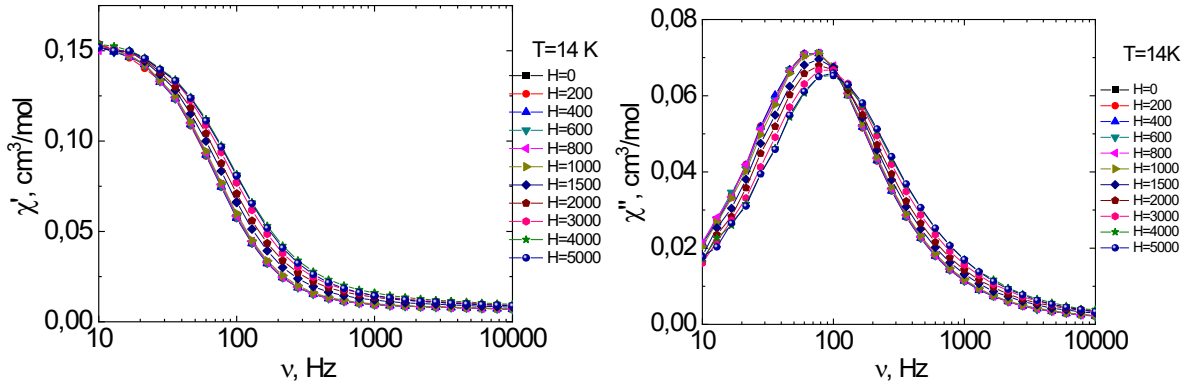

Figure S35. In-phase (χ') and out-of-phase (χ'') ac magnetic susceptibility for $[Co(FPzOx)_3(BC_6H_5)Cl]$ measured at varied external magnetic field at 14 K. The solid lines are visual guides.

Table S8. Relaxation times for the complex $[Co(FPzOx)_3(BC_6H_5)Cl]$ in zero and 1000 Oe dc field .

T K	τ, s (H = 0 Oe)	τ, s (H= 1000 Oe)
10	0.0179	0.01765
12	0.00606	0.00594
14	0.0023	0.00223
16	7.81E-04	7.24E-04
18	2.39E-04	2.11E-04
20	7.61E-05	6.46E-05
22	2.73E-05	2.28E-05

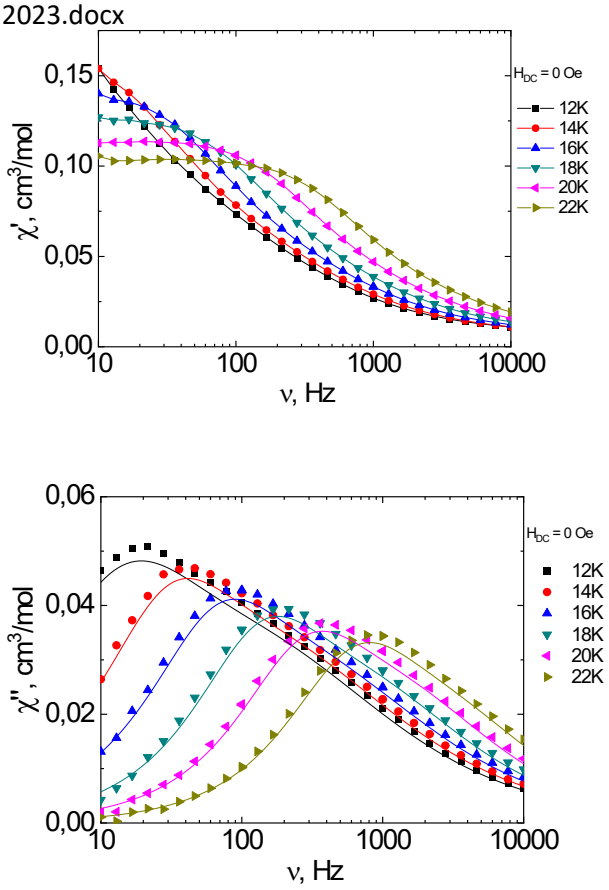

Figure S36. In-phase (χ') and out-of-phase (χ'') ac magnetic susceptibility for $[Co(PzOx)_3(BC_6H_5)I]$ measured at zero dc magnetic field and at various temperatures. The solid lines for out-of-phase χ'' magnetic susceptibility display approximation by the generalized Debye model.

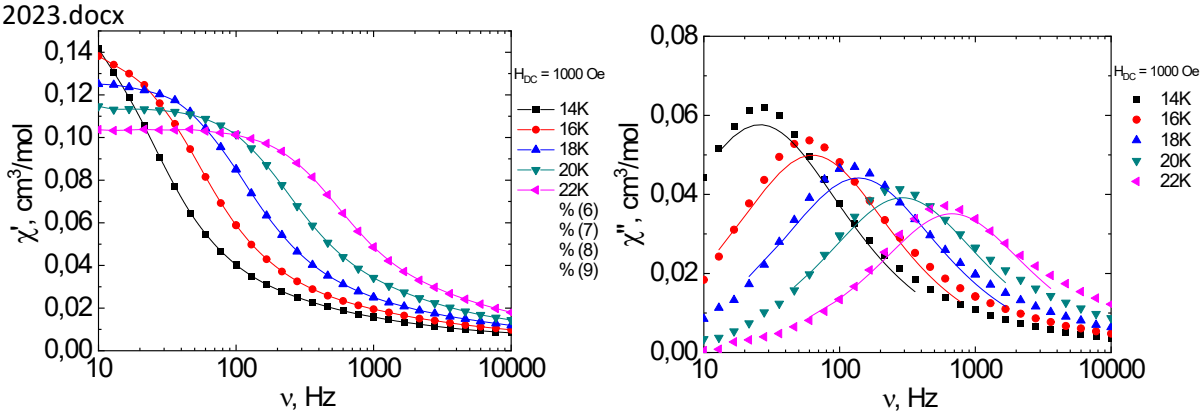

Figure S37. In-phase (χ') and out-of-phase (χ'') ac magnetic susceptibility for $[Co(PzOx)_3(BC_6H_5)I]$ measured at 1000 Oe dc external magnetic field and at various temperatures. The solid lines for out-of-phase χ'' magnetic susceptibility display approximation by the generalized Debye model.

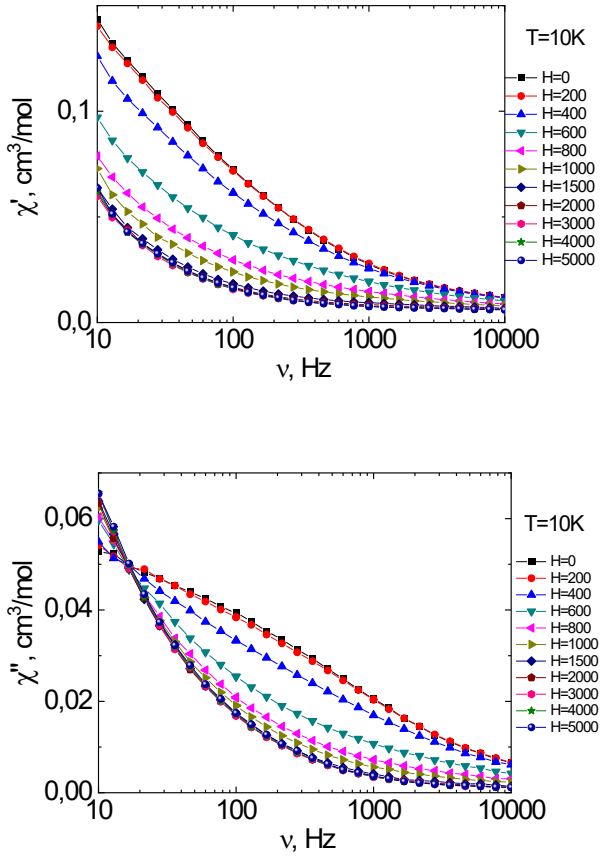

Figure S38. In-phase (χ') and out-of-phase (χ'') ac magnetic susceptibility for $[Co(PzOx)_3(BC_6H_5)I]$ measured at varied external magnetic field at 10 K. The solid lines are visual guides.

Table S9. Relaxation times for the complex $[Co(PzOx)_3(BC_6H_5)I]$ in zero and 1000 Oe dc field (LF - low frequeny peak, HF – high frequency peak).

T K	τ, s (H = 0 Oe), LF	τ, s (H = 0 Oe), HF	τ, s (H= 1000 Oe)
10	n/d	n/d	9.00E-03
12	1.14E-02	8.88E-04	0.00369
14	5.15E-03	7.90E-04	0.00615
16	2.35E-03	3.98E-04	0.00252
18	1.13E-03	1.78E-04	0.00116
20	5.54E-04	9.48E-05	5.48E-04
22	2.44E-04	4.44E-05	2.37E-04

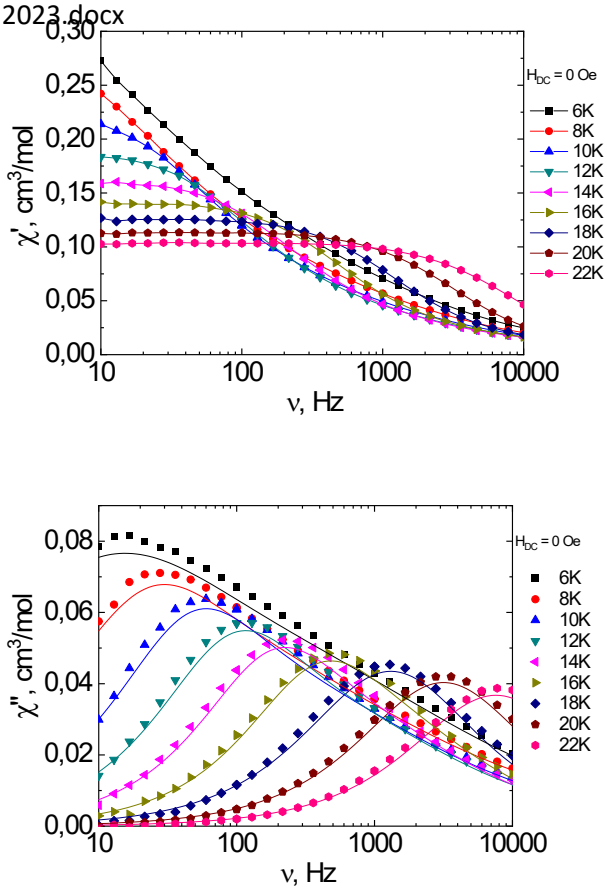

Figure S39. In-phase (χ') and out-of-phase (χ'') ac magnetic susceptibility for $[Co(PzOx)_3(BC_6H_5)Br]$ measured at zero dc magnetic field and at various temperatures. The solid lines for out-of-phase χ'' magnetic susceptibility display approximation by the generalized Debye model.

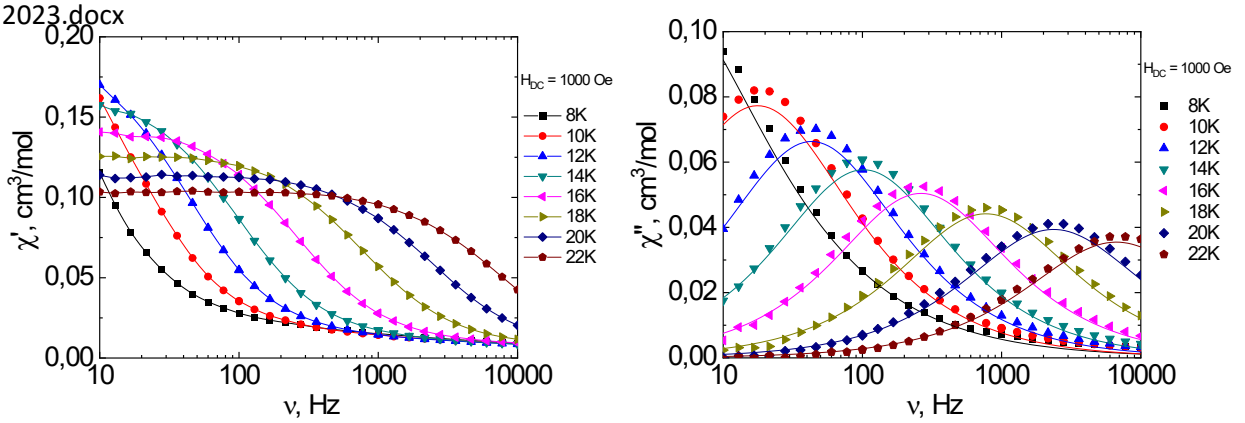

Figure S40. In-phase (χ') and out-of-phase (χ'') ac magnetic susceptibility for $[Co(PzOx)_3(BC_6H_5)Br]$ measured at 1000 Oe dc magnetic field and at various temperatures. The solid lines for out-of-phase χ'' magnetic susceptibility display approximation by the generalized Debye model.

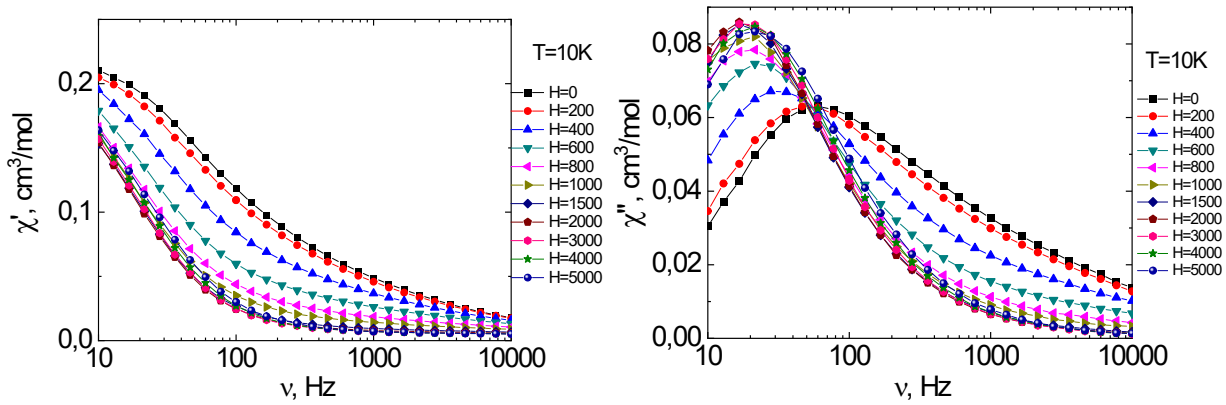

Figure S41. In-phase (χ') and out-of-phase (χ'') ac magnetic susceptibility for $[Co(PzOx)_3(BC_6H_5)Br]$ measured at varied dc magnetic field at 10 K. The solid lines are visual guides.

Table S10. Relaxation times for the complex $[Co(PzOx)_3(BC_6H_5)Br]$ in zero and 1000 Oe dc field (LF - low frequeny peak, HF – high frequency peak).

T K	τ, s (H = 0 Oe), LF	τ, s (H = 0 Oe), HF	τ, s (H= 1000 Oe)
6	0.01443	2.54E-04	n/d
8	0.00704	0.0012	n/d
10	0.00165	4.40E-04	9.00E-03
12	8.45E-04	2.07E-04	0.00369
14	3.90E-04	1.22E-04	1.56E-03
16	1.82E-04	7.27E-05	6.03E-04
18	1.45E-04	5.81E-05	2.06E-04
20	5.03E-05	4.18E-05	6.74E-05
22	2.10E-05		2.39E-05

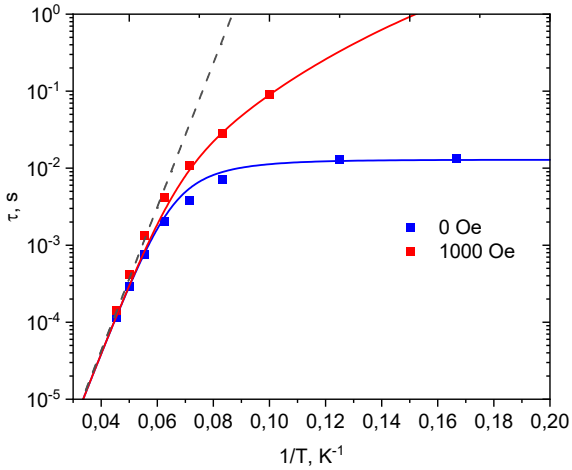

Figure S42. Relaxation times for $[Co(PzOx)_3(BC_6H_5)Cl]$ at 0 and 1000 Oe constant magnetic field measured at various temperatures. The solid lines represent approximation according to eq. 4 with parameters from table S5. The dashed line represents Orbach contribution with parameters from table S5.

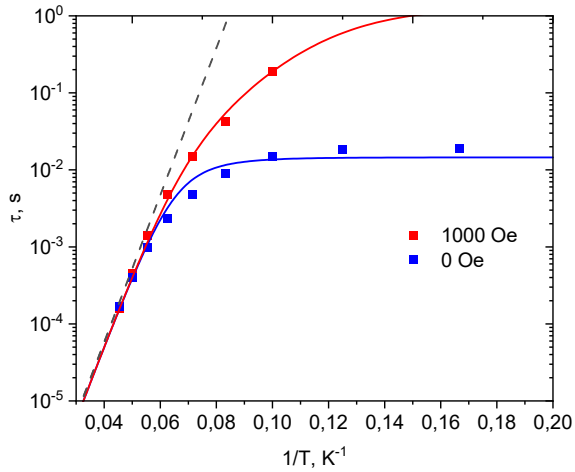

Figure S43. Relaxation times for $[Co(PzOx)_3(BC_6H_5)Cl] \cdot (CH_3)_2CO$ at 0 and 1000 Oe constant magnetic field measured at various temperatures. The solid lines represent approximation according to eq. 4 with parameters from table S5. The dashed line represents Orbach contribution with parameters from table S5.

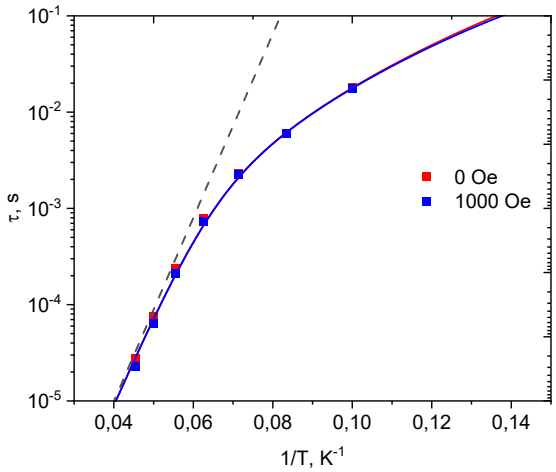

Figure S44. Relaxation times for $[Co(FPzOx)_3(BC_6H_5)Cl]$ at 0 and 1000 Oe constant magnetic field measured at various temperatures. The solid lines represent approximation according to eq. 4 with parameters from table S5. The dashed line represents Orbach contribution with parameters from table S5.

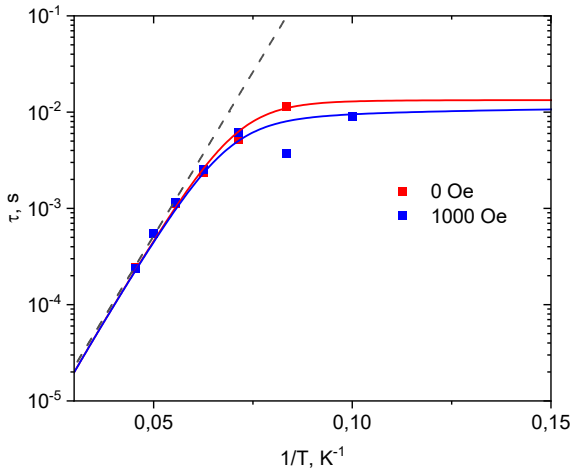

Figure S45. Relaxation times for $[Co(PzOx)_3(BC_6H_5)I]$ at 0 and 1000 Oe constant magnetic field measured at various temperatures. The solid lines represent approximation according to eq. 4 with parameters from table S5. The dashed line represents Orbach contribution with parameters from table S5.

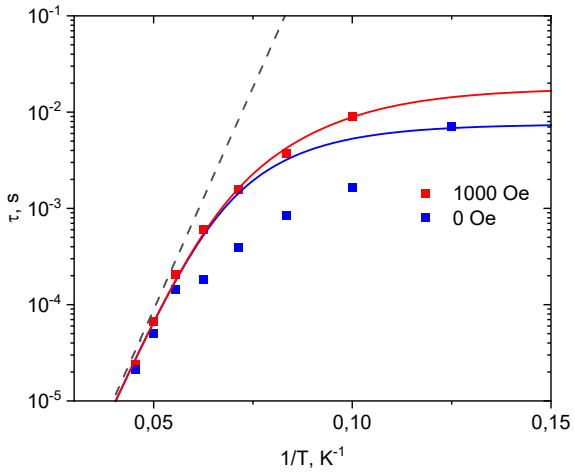

Figure S46. Relaxation times for $[Co(PzOx)_3(BC_6H_5)Br]$ at 0 and 1000 Oe constant magnetic field measured at various temperatures. The solid lines represent approximation according to eq. 4 with parameters from table S5. The dashed line represents Orbach contribution with parameters from table S5.

References Supporting Information

[S1]. O. A. Varzatskii, S. V. Kats (Menkach), L. V. Penkova, S. V. Volkov, A. V. Dolganov, A. V. Vologzhanina, Y. N. Bubnov, Y. Z. Voloshin, Cage metal complexes: synthesis, X-ray structure, and spectral and redox behavior of the first hybrid iron(II) clathrochelatoscorpionate and its pyrazoloxime-armed macrocyclic intermediate, *Eur. J. Inorg. Chem*., 2013, 1987–1992, DOI: 10.1002/ejic.201201545.

[S2]. T. Nyui, T. Nogamia, T. Ishida, Organic kagomé lattice consisting of trimeric pyrazole and oxime supramolecular synthons from 3-pyrazolecarboxaldoxime, *CrystEngComm*, 2005, **7**, 612–615, DOI: 10.1039/B512977J.

[S3] M. Wojdyr, Fityk: a general-purpose peak fitting program, *J. Appl. Cryst*., 2010, **43**, 1126–1128, DOI: 10.1107/S0021889810030499.

[S4]. (a) O. A. Varzatskii, L. V. Penkova, S. V. Kats, A. V. Dolganov, A. V. Vologzhanina, A. A.Pavlov, V. V. Novikov, A. S. Bogomyakov, V. N. Nemykin, Y. Z. Voloshin, Chloride ion-aided self-assembly of the pseudo-clathrochelate metal tris-pyrazoloximates, *Inorg. Chem*., 2014, **53**, 3062–3071, DOI: 10.1021/ic4029047

[S5]. N. Schoorl, L.M. van den Berg, *Chem.Centr. ii*, 1905, 1623.

[S6]. A. S. Belov, A. V. Vologzhanina, Y. V. Fedorov, E. V. Kuznetsov, Y. Z. Voloshin, Unexpected transformation of mono- to bis-macrobicyclic dimethylglyoximate framework in a chloroform solution: photochemical, MALDI-TOF MS and X-ray diffraction studies, *Inorg. Chem. Commun*., 2013, **35**, 242 – 246, DOI: 10.1016/j.inoche.2013.06.036.

[S7]. (a) Y. Z. Voloshin, N. A. Kostromina, R. Krämer, *Clathrochelates: synthesis, structure and properties*, Elsevier, 2002; (b) Y. Z. Voloshin, I. G. Belaya, R. Krämer, *Cage metal complexes: clathrochelates revisited*, Springer,

2017; (c) Y. Z. Voloshin, O. A. Varzatskii, I. I. Vorontsov, M. Yu. Antipin, Tuning a Metal's Oxidation State: The Potential of Clathrochelate Systems, *Angew. Chem. Int. Ed*., 2005, **44**, 3400–3402, DOI: 10.1002/anie.200463070; (d) O. Pantani, S. Naskar, R. Guillot, P. Millet, E. Anxolabehere-Mallart, and A. Aukauloo, Cobalt clathrochelate complexes as hydrogen-producing catalysts, *Angew. Chem. Int. Ed*., 2008, **47**, 9948, DOI: 10.1002/anie.200803643; (e) Y. Z. Voloshin, O. A. Varzatskii, V. V. Novikov, N. G. Strizhakova, I. I. Vorontsov, A. V. Vologzhanina, K. A. Lyssenko, G. V. Romanenko, M. V. Fedin, V. I. Ovcharenko, Y. N. Bubnov, Tris-dioximate cobalt(I, II, and III) clathrochelates: stabilization of different oxidation and spin states of an encapsulated metal ion by ribbed functionalization, *Eur. J. Inorg. Chem*., 2010, 5401–5415, DOI: 10.1002/ejic.201000444; (f) D. I. Kochubey, V. V. Kaichev, A. A. Saraev, S. V. Tomyn, A. S. Belov, Y. Z. Voloshin, Combined XANES and XPS study of the electrocatalytically active cobalt(I) cage complexes and the clathrochelate cobalt(II)- and cobalt(III)-containing precursors and analogs, *J. Phys. Chem. C*., 2013, **117**, 2753 – 2759, DOI: 10.1021/jp3085606; (g) G. E. Zelinskii, A. A. Pavlov, A. S. Belov, I. G. Belaya, A. V. Vologzhanina, Y. V. Nelyubina, N. N. Efimov, Y. V. Zubavichus, Y. N. Bubnov, V. V. Novikov, Y. Z. Voloshin, A new series of cobalt and iron clathrochelates with perfluorinated ribbed substituents, *ACS Omega*, 2017, 2, 6852 – 6862, DOI:10.1021/acsomega.7b01088; (h) Y. Z. Voloshin, V. V. Novikov, Y. V. Nelyubina, A. S. Belov, D. M. Roitershtein, A. Savitsky, A. Mokhir, J. Sutter, M. E. Miehlich and K. Meyer, *Chem. Commun*., 2018, **54**, 3436–3439, DOI: 10.1039/C7CC09611A; (i) A. J. Campanella, T. M. Ozvat, J. M. Zadrozny, Ligand design of zero-field splitting in trigonal prismatic Ni(II) cage complexes, *Dalton Trans*., 2022, **51**, 3341–3348, DOI: 10.1039/d1dt02156g; (j) Y. Wei, Y. Dong, W. Sun, Q. Hou, Q. Shi, X. Lan, Phase behavior and heat capacity of alkylboron-capped cobalt(II) and nickel(II) clathrochelates, *Thermochim. Acta*, 2022, **716**, 179304, DOI: 10.1016/j.tca.2022.179304; (k) A. S. Belov, V. V. Novikov, A. V. Vologzhanina, A. A. Pavlov, A. S. Bogomyakov, Y. V

Zubavichus, R. D. Svetogorov, G. E. Zelinskii, Y. Z. Voloshin, Template synthesis, crystal polymorphism and spin crossover behavior of the adamantylboron-capped cobalt(II) tris-dioximate hexachloroclathrochelate and its unexpected (photo)chemical transformation into unusual $Co^{III}Co^{II}Co^{III}$-trinuclear dodecachloro-bis-macrobicyclic derivative, *Dalton Trans*., 2023, **52**, 347–359, DOI: 10.1039/D2DT03300C; (l) R. Thaler, H. Kopacka, K. Wurst, T. Müller, F. R. Neururer, S. Hohloch, P. Lippmann, I. Ott, B. Bildstein, Clathrochelate Complexes Containing Axial Cymantrene and Tromancenium Moieties, *Eur. J. Inorg. Chem.*, 2023, DOI: 10.1002/ejic.202300368; (m) D. V. Balatskiy, A. S. Chuprin, S. V. Dudkin, L. F. Desdín-García, A. L. Corcho-Valdés, M. Antuch, V. M. Buznik, S. Yu. Bratskaya, Y. Z. Voloshin, ^{57}Fe Mössbauer and DFT study of the electronic and spatial structures of the iron(II) (pseudo)clathrochelates: the effect of ligand field strength, *Phys.Chem.Chem.Phys*., 2023, **25**, 18679–18690, DOI: 10.1039/d3cp01887c (hot article); (n) I. Klemt, O. Varzatskii, R. Selin, S. Vakarov, V. Kovalska, R. Bilyy, Y. Voloshin, I. Cossío Cuartero, A. Hidalgo, B. Frey, I. Becker, B. Friedrich, R. Tietze, R. P. Friedrich, C. Alexiou, E.-L. Ursu, A. Rotaru, I. Solymosi, M. E. Pérez-Ojeda, A. Hirsch, A. Mokhir, 3D-shaped binders of unfolded proteins inducing cancer cell specific endoplasmic reticulum stress in vitro and in vivo, J. Am. Chem. Soc., 2023, DOI: 10.1021/jacs.3c08827.

[S8]. A. S. Belov, Y. Z. Voloshin, A. A. Pavlov, Y. V. Nelyubina, S. A. Belova, Y. V. Zubavichus, V. V. Avdeeva, N. Efimov, E. A. Malinina, K. Y. Zhizhin, N. T. Kuznetsov, Solvent-induced encapsulation of cobalt(II) ion by a boron-capped tris-pyrazoloximate, *Inorg.Chem*., 2020, **59**, 9, 5845–5853, DOI: 10.1021/acs.inorgchem.9b03335;

[S9]. (a) L. P. Hammett, *Physical Organic Chemistry. Reaction Rates*, Equilibria and Mechanism, McGraw-Hill Book Company, 1970; (b) C. D. Johnson. *The Hammett Equation*, Cambridge University Press, 1980; (c) C. Hansch, A. Leo,

R. W. Taft, A survey of Hammett substituent constants and resonance and field parameters, *Chem. Rev.,* 1991, **91**, 165 – 195.

[S10]. Yu.V. Nelyubina, A.S. Belov, S.A. Belova, Y.V. Zubavichus, S.Malinkin, Y.Z. Voloshin, Unexpected side products of chemical transformations in cobalt(II) pseudoclathrochelates: an X-ray diffraction study, *Chemistry Select*, 2020, 5, 12307– 12312.

[S11]. S. V. Kats, O. V. Severynovskaya, O. A. Varzatskii, E. G. Lebed, V. A. Pavlenko, The peculiarities of ionization, fragmentation and association (macrobicyclization) of pseudoclathrochelate tris-pyrazoloximates of zinc(II), cobalt(II), iron(II) and manganese(II), *Macroheterocycles*, 2015, **8**, 314–320, DOI: 10.6060/mhc150979l.

[S12]. N. F. Chilton, R. P. Anderson, L. D. Turner, A. Soncini, K. S. Murray, PHI: A powerful new program for the analysis of anisotropic monomeric and exchange-coupled polynuclear d- and f-block complexes, *Computation Chem*., 2013, **34**, 1164–1175, DOI: 10.1002/jcc.23234.

[S13]. O. A. Varzatskii, L. V. Penkova, S. V. Kats (Menkach), A. V. Dolganov, A. V. Vologzhanina, A. A.Pavlov, V. V. Novikov, A. S. Bogomyakov, V. N. Nemykin, Y. Z. Voloshin, Chloride ion-aided self-assembly of the pseudo-clathrochelate metal tris-pyrazoloximates, *Inorg. Chem*., 2014, **53**, 3062–3071, DOI: 10.1021/ic4029047.